

# ELECTROPRODUCTION OF LIGHT QUARK BARYONS

Volker D. Burkert

Continuous Electron Beam Accelerator Facility,  
12000 Jefferson Avenue, Newport News, Virginia 23606, USA.

## Abstract.

The status of electromagnetic excitation of light quark (u, d) baryon states is reviewed and confronted with results of calculations within the framework of microscopic models of the baryon structure and the photon - baryon coupling. Prospects for a qualitative improvement of our knowledge in this sector using photon and electron beams at the new, intermediate energy continuous wave (CW) electron machines are discussed.

## 1. INTRODUCTION

Understanding the structure of hadrons in terms of the fundamental interaction of the constituent quarks and gluons is one of the challenges in strong interaction physics. The study of hadron spectroscopy using hadronic probes has taught us a great deal about the excitation spectra and the hadronic properties of some of the excited baryon states. However, a complete understanding of the internal structure of baryons can only be accomplished using the electromagnetic interaction as a probe. In this talk, I will focus on the electromagnetic transition between non-strange baryon states. This sector received much attention in the early 1970's after the development of the first dynamical quark models. However, experimental progress was slow, partly because of the low rates associated with electromagnetic interactions, and partly because of the lack of guidance by theoretical models that went beyond the simplest quark models. It was difficult for experiments to achieve the precision needed for a detailed analysis of the entire resonance region in terms of the fundamental photocoupling amplitudes over a large range in momentum transfer.

More realistic models were developed after the major electron accelerators used in these studies had been shut down in the wake of the  $J/\psi$  discovery in 1974.

With the construction of CW electron accelerators in the GeV and multi-GeV region, this situation is changing in a significant way. For example, use of large acceptance detectors at high luminosities of up to  $10^{34} \text{ cm}^{-2} \text{ sec}^{-1}$  will become feasible, allowing measurement of several reaction channels simultaneously<sup>1</sup>, over a large kinematic range, and with statistical accuracy comparable to that achieved with hadronic probes. Moreover, with 100% duty cycle, intense electron beams, high statistics coincidence measurements can be conducted for exclusive channels with small cross sections. In fact, to a large degree the statistics will not be limited by the luminosity achievable in these measurements but rather by the speed of the data acquisition system and the data analysis process. It is interesting to note that hadronic reactions will no longer enjoy their traditional rate advantage over electromagnetic processes. This will bring to bear the full power of the electromagnetic interaction as a probe of the internal structure of hadrons and the strong interaction.

The interaction of the baryon constituents, quarks and gluons, is generally perceived to be described by QCD, the theory of strong interactions. However, solutions of this theory in the non-perturbative domain are extremely difficult to achieve. The lattice gauge theory offers the best hope for exact calculations, but results seem to be far in the future. Thus, models will continue to play an important role. Microscopic models that utilize QCD relate the internal baryon structure to the strong interaction of the confined constituents, quarks and gluons. Probing baryons with photons and electrons will give us insight into this fundamental interaction. This is the main thrust of experiments using the electromagnetic probe. As we are entering into a new era of experiments exploiting the electromagnetic probe, it may be appropriate to review, in some detail, the status of the field. This article is organized as follows. Before reviewing the experimental status of electromagnetic transitions of baryons resonances, I briefly summarize the status of light quark baryon spectroscopy in section 2, and point to some of the problems, that need to be addressed experimentally. In section 3, I discuss some aspects of what we have learned about the baryon structure from inclusive electron scattering in the nucleon resonance region, and what we may learn by fully exploiting the power of spin polarized beams and polarized nucleon targets. In section 4 I discuss what has been learned from exclusive electroproduction of low mass nucleon resonances. In section 5, some new and old physics topics that need to be resolved are discussed. In section 6, some experimental aspects are addressed.

## 2. SUMMARY OF LIGHT QUARK BARYON SPECTROSCOPY

In the course of the past decade, very little has happened in experimental light quark baryon spectroscopy, and, considering its importance for the understanding of the structure of baryons, it appears to be still in its infancy. The 1990 edition of the Review of Particle Properties<sup>2</sup> (RPP) lists 23 established  $N^*$  or  $\Delta$  states, and about as many candidate states with insufficient experimental evidence. However, this is only a small fraction of the states predicted by the most accepted QCD inspired quark models. Most of the information we have on baryons states is the result of partial wave analyses of elastic pion-nucleon scattering measurements  $\pi N \rightarrow \pi N$ . The methods used, the results of the analyses, and remaining problems have been discussed in a recent review<sup>3</sup>.

The non-relativistic, QCD inspired quark model<sup>4</sup> and its relativized version<sup>5</sup> allow the association of all established states with a level in the  $SU(6) \times O(3)$  representation. The ground states and all states associated with the  $[70, 1^-]_1$  super multiplet have been observed experimentally. However, several of the  $N=2$  states, and most of the  $N=3$  and  $N=4$  states have not been seen in  $\pi N \rightarrow \pi N$  reactions. Figure 2.1 summarizes the experimental situation for the  $N=2$  and  $N=3$  super multiplets. After overall adjustments of the center-of-mass excitation energies, the predicted levels for most of the states are in fair agreement with the measured masses. There are a few exceptions, where the discrepancies are significantly beyond the experimental errors. The  $D_{35}(1930)$  is such a case. The experimental mass is 1890 to 1960 MeV. The model of Forsyth and Cutkosky<sup>7</sup> predicts a  $D_{35}$  state at 2131 MeV, and the model of Capstick and Isgur<sup>5</sup> at 2030 MeV. The fact that there is only fair agreement between experimental resonance masses and masses predicted in quark model calculations is not necessarily alarming. Dynamic effects, such as pion re-scattering may contribute to shifting the resonance masses. These effects have not been taken into account in current quark model calculations. An intriguing observation is the apparent clustering of resonance masses. Many states appear to cluster in certain mass regions. For example, six  $N^*$  states and two  $\Delta$  states cluster in a mass range from 1620 to 1720 MeV. There are another six  $\Delta$  states with masses from 1900 to 1950 MeV. Is this clustering accidental, or is there a mechanism at work that pulls these states together? At present we don't know. There have been speculations that the effect might be due to phase locking in strongly inelastic resonance decays<sup>8</sup>.

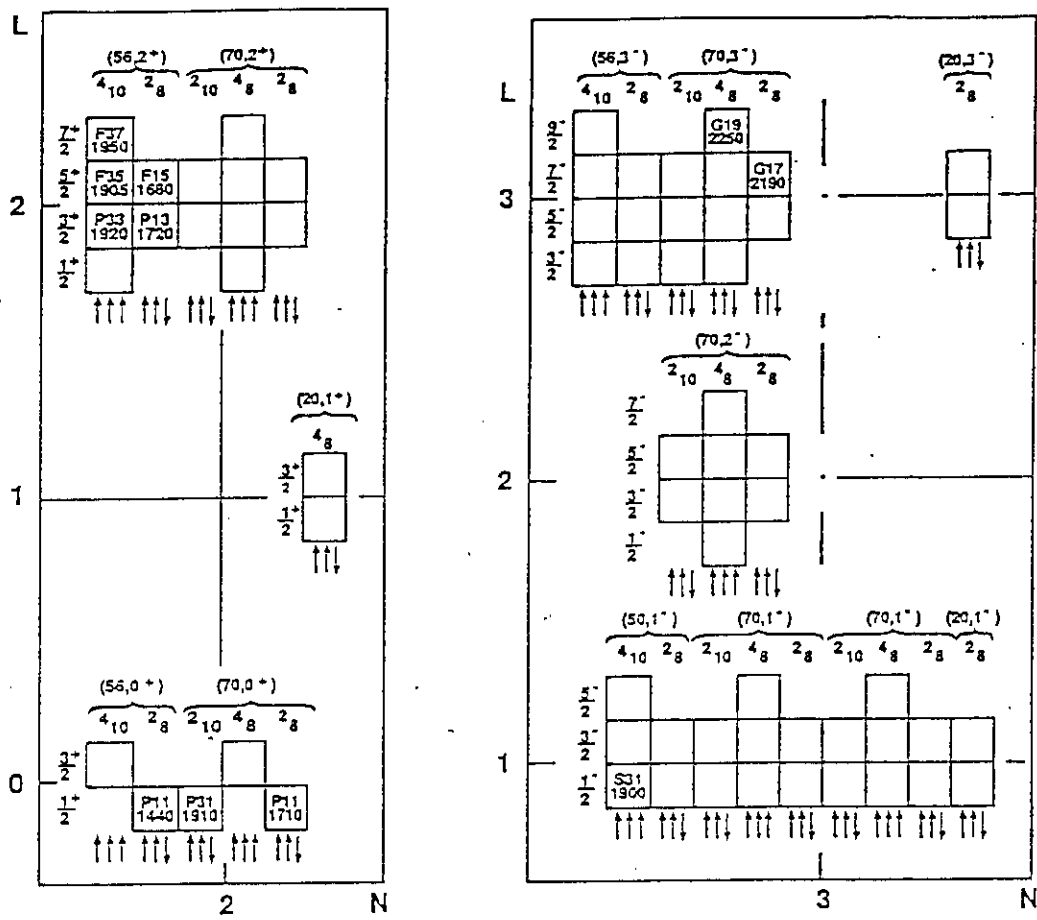


Figure 2.1 Experimental status of the  $N=2$  and  $N=3$   $q^3$  model states. The graph is from Ref.[6] (slightly modified).

Experimental uncertainties in the widths of many states are large (Figure 2.2). In the case of the  $P_{11}(1440)$ , the uncertainty is nearly a factor of 3. The  $P_{11}(1440)$  is listed by the PDG as a single well established resonance. This conclusion is based upon the Karlsruhe-Helsinki<sup>9</sup> and the CMU-LBL<sup>10</sup> partial wave analyses. The significantly different values found for the width of this state in the two analyses is disturbing. Clearly, the analysis of this energy region is complicated due to the opening up of the  $\pi\Delta(1232)$  channel and the large branching ratio of the  $P_{11}(1440)$  into this channel. In a more recent analysis by the VPI group<sup>11</sup> which included new  $\pi N$  data in the energy region of the  $P_{11}(1440)$ , two poles were found in the complex energy plane. This result led to speculations about a possible splitting of

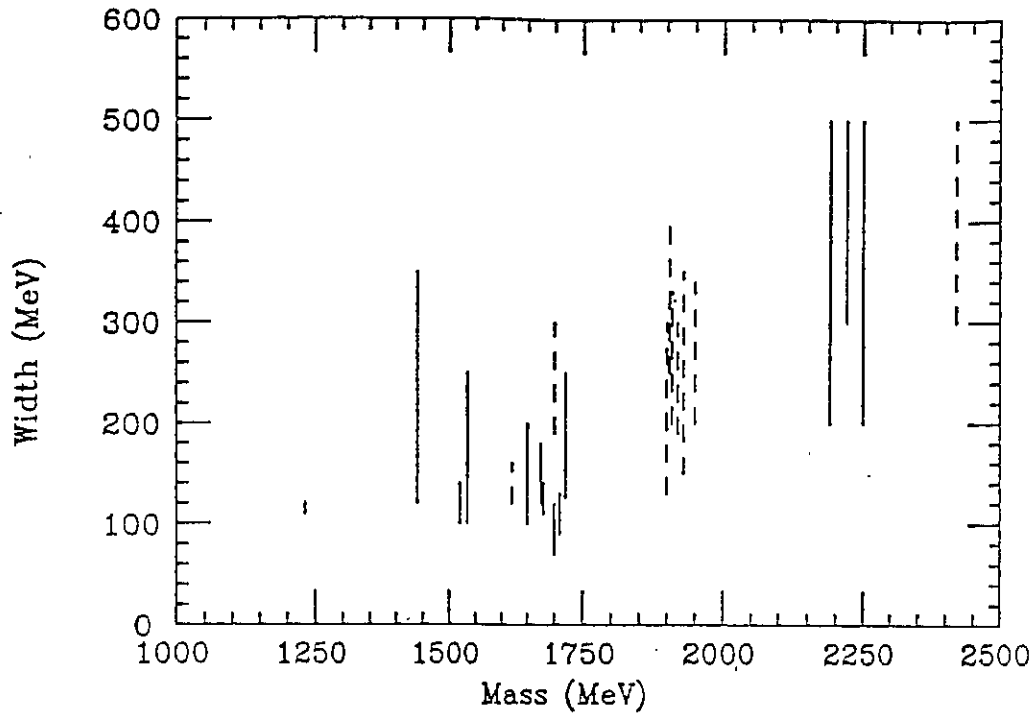


Figure 2.2 Widths (including experimental uncertainties) of non-strange baryon states.

the Roper into two states. However, arguments have been presented<sup>12</sup> that such a double pole might just be what is expected from single resonances in the presence of open inelastic channels. While there is no conclusive evidence towards either one of these interpretations, recent  $\pi N \rightarrow \pi N$  data from LAMPF and Leningrad<sup>13</sup> in the energy regime of the  $P_{11}$  may justify a new analysis of the K-H or CMU-LBL type to shed more light on this problem.

### 2.1 Missing Baryon States

Koniuk and Isgur<sup>14</sup> have suggested that the problem of the missing states in the  $q^3$  quark model may be an experimental problem and related to the lack of data in the inelastic channels. They predict most of the missing states to largely decouple from the  $\pi N$  channel. The  $\pi N \rightarrow \pi N$  process becomes rather ineffective in searching for these states. Many of the  $N=2$  and  $N=3$  states are predicted to couple strongly to  $\Delta\pi$ ,  $\rho N$ , and  $\omega$ . If the  $\pi N$  channel does not totally decouple from the resonance, the process  $\pi N \rightarrow \pi\pi N$  may offer a better chance for detecting these states. Analyzing this channel in bubble chamber data, Manley<sup>15</sup> found evidence

State	$\pi N$	$\eta N$	$N\pi\pi$
$P_{11}(1710)$	10-20	$\sim 25$	$\leq 50$
$P_{13}(1720)$	10-20	$\sim 3.5$	$\leq 75$
$G_{17}(2190)$	$\sim 14$	$\sim 3$	?
$H_{19}(2220)$	$\sim 18$	$\sim 0.5$	?
$G_{19}(2250)$	$\sim 10$	$\sim 2$	?
$I_{11,1}(2600)$	5	$\sim 2$	?
$P_{31}(1910)$	15-25	-	$\leq 75$
$P_{33}(1920)$	15-20	-	?
$D_{35}(1950)$	5-15	-	not seen
$F_{37}(1710)$	35-45	-	$\leq 40$
$H_{3,11}(2420)$	5-15	-	?

for one of the predicted states, a  $F_{35}$  with a mass around 2000 MeV. In case the decoupling from the  $\pi N$  channel is nearly complete, electromagnetic transitions may be the only way to search for these states. Obviously, our picture of baryon structure could change dramatically if these states do not exist. An extensive search for at least some of these states is therefore important and urgent. The quark cluster model<sup>16</sup> and the algebraic model of Iachello<sup>17</sup> can accommodate the known baryon spectrum, but predict a fewer number of states. In these models the quarks are not in a spherically symmetric configuration but rather in a diquark-quark configuration (Figure 2.3). Electroproduction of nucleon resonances should be a very sensitive tool to distinguish between these alternative configurations.

Inelastic channels are not well determined experimentally, due to the lack of sufficiently detailed data in the  $\pi N \rightarrow \pi\pi N$ ,  $\pi N \rightarrow \pi\pi\pi N$ , and  $\pi N \rightarrow \eta N$  channels (table 2.1). The lack of knowledge of fundamental resonance properties has serious

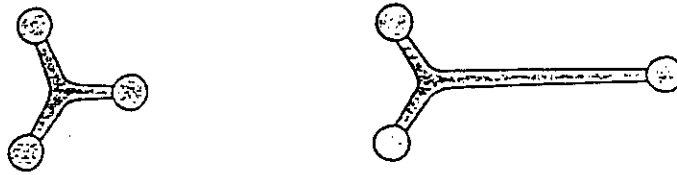


Figure 2.3 Spherically symmetric  $q^3$ , and non-spherical  $q^2 - q$  baryon configuration.

consequences regarding systematic uncertainties in the extraction of photocoupling amplitudes, where properties of the hadronic vertex are needed as input.

Another category of baryons about which we have no experimental information are the gluonic excitations or hybrids  $q^3 G$ . These states have been discussed within the framework of the bag model<sup>18,19</sup>. Low lying states like  $P_{11}(1440)$ ,  $P_{13}(1540)$ ,  $P_{31}(1550)$ ,  $P_{33}(1600)$ ,  $P_{11}(1700)$  are possible candidates for gluonic excitations. The problem is how to distinguish gluonic excitation from regular  $q^3$  excitations. Some of the hybrid states, e.g. the  $P_{13}(1540)$ , or the  $P_{31}(1550)$  are not allowed in the  $q^3$  model, therefore their mere existence would already signal that the standard quark model cannot be complete. Experimental indications for these states are weak and have been found in inelastic channels only<sup>20</sup>. As we will discuss in section 5, measurements of the electromagnetic transition form factors are a powerful tool in determining the nature of these states.

### 3. INCLUSIVE ELECTRON SCATTERING

#### 3.1 Unpolarized inclusive cross section

The inclusive electron scattering cross section  $eN \rightarrow eX$  reveals a few broad bumps, clearly indicating the excitation of resonances in the mass region below 2 GeV (Figure 3.1). However, their broad widths and close spacing make it impossible to separate them in inclusive production reactions. Nonetheless, one can obtain some global information about the  $Q^2$  dependence of the dominant states, by subtracting some smooth non-resonant background contribution. This technique has been used by various groups<sup>23</sup>, most recently to study the photocoupling amplitudes of the prominent states at very high momentum transfers<sup>24,25</sup>.

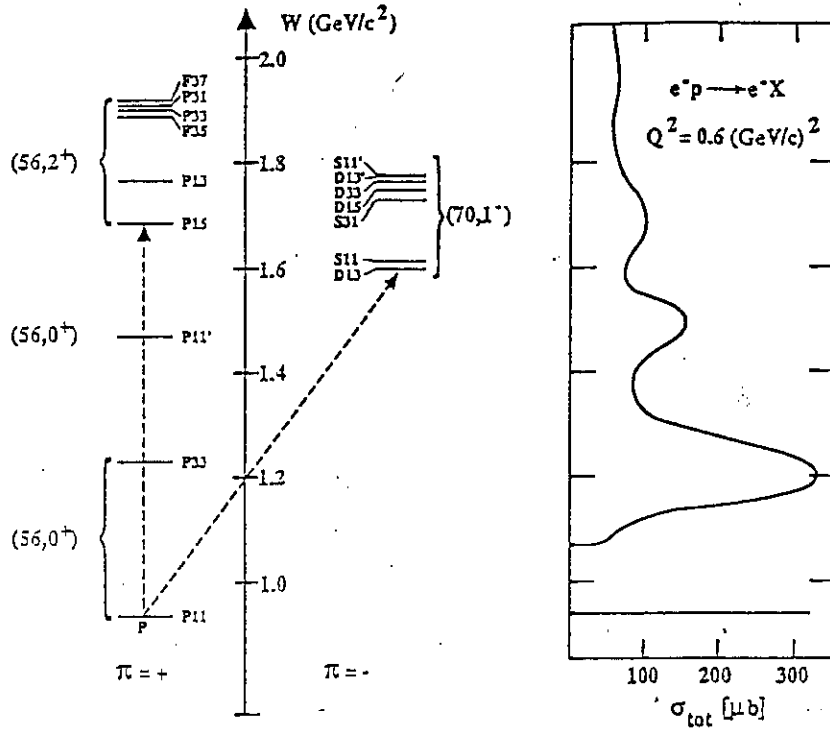


Figure 3.1 The nucleon resonances with masses below 2 GeV (left) and the shape of the inclusive cross section at  $Q^2 = 0.6 \text{ GeV}^2$  (right).

The inclusive unpolarized electron scattering cross section can be written as:

$$\frac{d\sigma}{d\Omega_e dE'_e} = \Gamma_T \cdot \sigma_{TOT} \quad (1)$$

$$\sigma_{TOT} = (\sigma_T + \epsilon\sigma_L) \quad (2)$$

where  $\Gamma_T$  is the virtual photon flux, and  $\epsilon$  describes the photon polarization.  $\sigma_T$  and  $\sigma_L$  are the transverse and longitudinal total absorption cross sections, respectively. The transverse total absorption cross section  $\sigma_T$  can be expressed in terms of the total absorption for helicity 1/2 and helicity 3/2, in the initial state photon-nucleon system.

$$\sigma_T = 1/2(\sigma_T^{1/2} + \sigma_T^{3/2}) \quad (3)$$

$\sigma_L$  is typically small. For example, in the deep inelastic region  $\sigma_L \simeq 0.15$  due to the primordial transverse momentum of the quarks inside the nucleon. In the resonance region, a significant  $\sigma_L$  could be evidence for non-quark degrees of freedom, such as photon absorption on spin-0 objects like pions or diquarks inside the nucleon.

Quark models predict small values of  $\sigma_L/\sigma_T$  for the resonance couplings, with possible exceptions for radial excitations, like the Roper  $P_{11}(1440)$ . Accurate separate measurements of  $\sigma_L$  and  $\sigma_T$  can therefore give important information about the internal structure of baryons.

The longitudinal part can be separated from the transverse part by measuring the  $\epsilon$  dependence of the total absorption cross section. This has been done for a few kinematical points only.  $\sigma_L$  was found to be relatively small throughout the resonance region, typically  $\sigma_L/\sigma_T \simeq 0.1 - 0.2$ . However, in some kinematic regions, considerably larger values cannot be excluded. The most accurate separation of  $\sigma_L$  and  $\sigma_T$  has been done at small  $Q^2$  in the  $\Delta(1232)$  region (Figure 3.2), with the result that no resonant longitudinal coupling was found. Of course, the total absorption cross section is not very sensitive to relatively small amplitudes since they enter in quadrature. Therefore, small resonant longitudinal contributions are not excluded, and measurements which are more sensitive to these terms should be carried out. Results of measurements at higher masses yield similarly small values (Figure 3.3).

In a simple ansatz one may assume an incoherent superposition of resonances and non-resonant background. At fixed  $Q^2$

$$\sigma_{TOT}(W) = \sigma_R(W) + \sigma_{NR}(W), \quad (4)$$

with a Breit-Wigner parameterization for the resonant part:

$$\sigma_R(W) = A_R \cdot \frac{\bar{Q}_R^{*2}}{\bar{Q}^{*2}} \cdot \frac{W_R^2 \cdot \Gamma \cdot \Gamma_T}{(W_R^2 - W^2)^2 + \Gamma^2 W_R^2}, \quad (5)$$

and a polynomial for the non-resonant contribution:

$$\sigma(W) = \sqrt{W - W_{thr}} \cdot \sum_{i=0}^m a_i \cdot (W - W_{thr})^i. \quad (6)$$

This expression provides an s-wave energy behaviour near threshold.  $\bar{Q}^*$  is the photon momentum in the hadronic rest frame. The least-square fit to the data yields  $A_R$ . For the higher mass resonances  $A_R$  is a superposition of different states with different widths, and different masses. The results are therefore ambiguous, and can give only indications of the global behaviour. The  $\Delta(1232)$ , however, is an isolated resonance, and the fit should yield information about the  $\Delta(1232)$  resonance only. Since  $\sigma_L$  is small in the  $\Delta$  region, the resonant cross section can be expressed in terms of the transverse transition form factors  $G_M^\Delta$  and  $G_E^\Delta$  only<sup>29</sup>:

$$\sigma_R \simeq \sigma_R^T = \frac{4\pi\alpha}{\Gamma} \cdot \frac{|\bar{Q}_L|^2}{W(W^2 - M^2)} \cdot (|G_M^\Delta|^2 + 3|G_E^\Delta|^2) \quad (7)$$

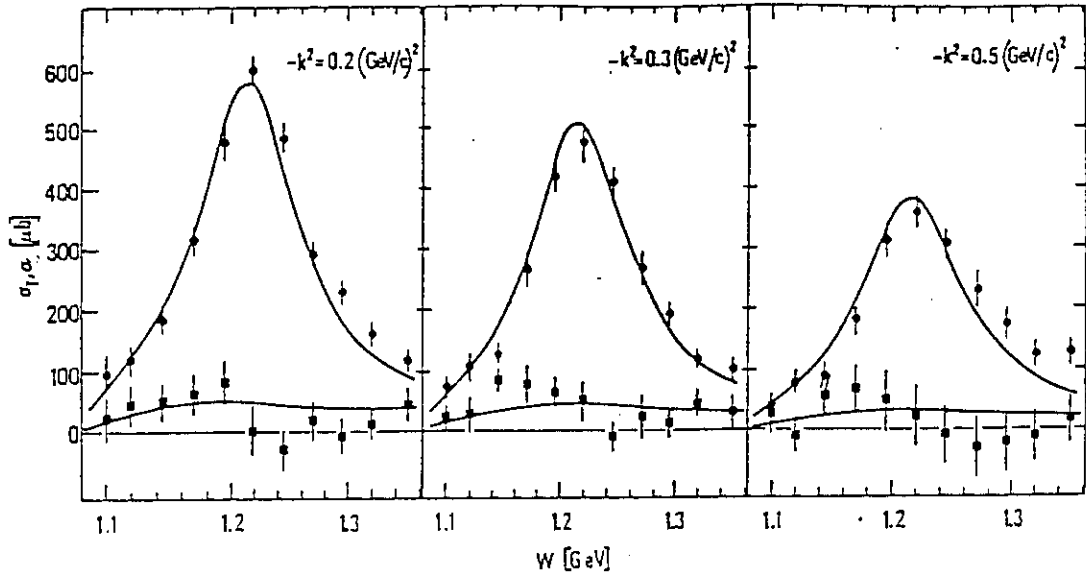


Figure 3.2 Transverse and longitudinal cross section in the  $\Delta(1232)$  region. Measurement from Bonn<sup>26</sup>.

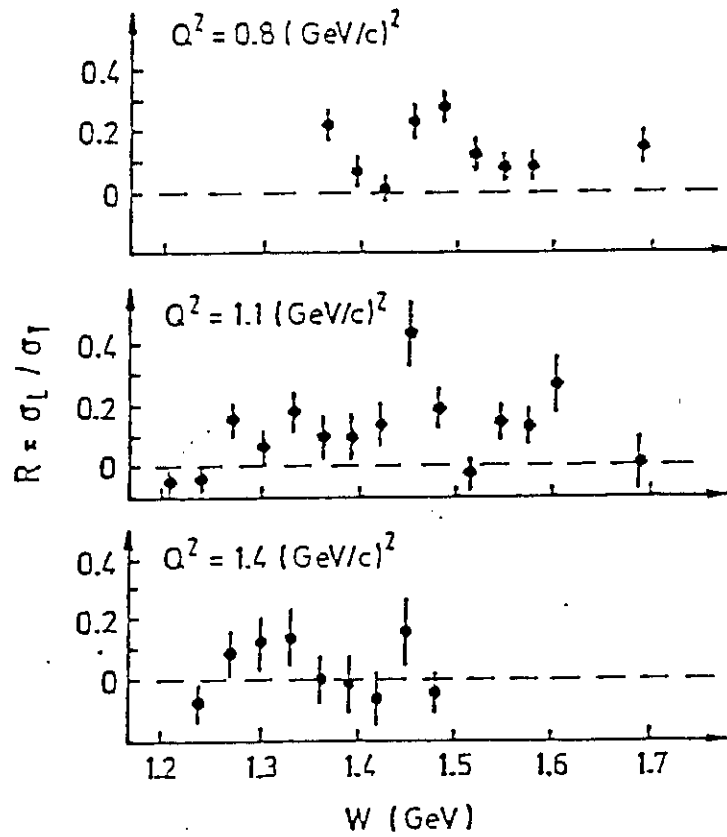


Figure 3.3 Ratio  $\sigma_L/\sigma_T$  in the resonance region<sup>27</sup>.

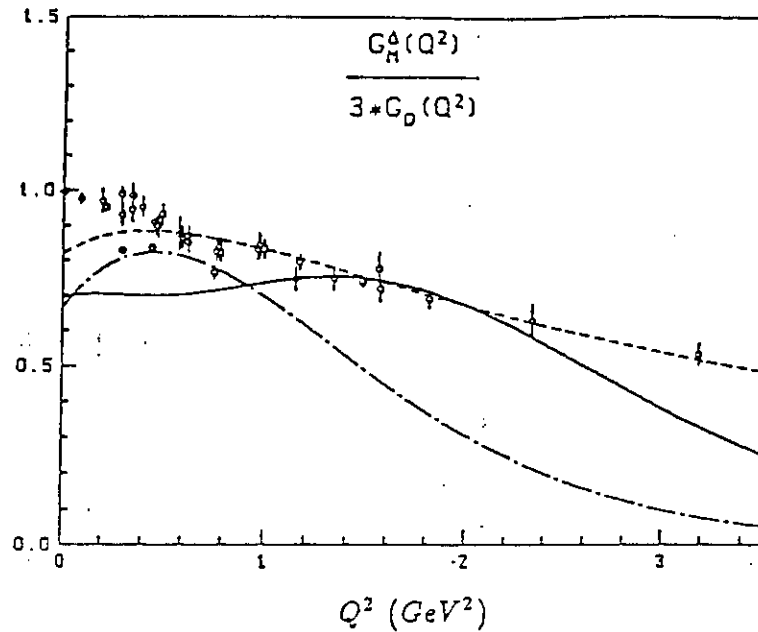


Figure 3.4 The magnetic transition formfactor  $G_M^\Delta$  normalized to the dipole formfactor. The curves are results of quark model calculations<sup>29,42</sup>.

where  $\vec{Q}_L$  is the photon momentum vector in the lab system. If  $G_E^\Delta$  is small, which, as we shall see later is the case for moderate values of  $Q^2$ , one can determine  $|G_M^\Delta|$ . A compilation of the results from various groups is shown in Figure 3.4. The comparison with quark models demonstrates a longstanding problem: at the photon point, quark models underestimate the magnetic multipole transition amplitude by 20 to 30%.

A detailed discussion of the high  $Q^2$  results, in particular for the higher mass resonances, was presented during the lecture series by C. Carlson<sup>24</sup>. I will therefore not discuss this aspect here.

### 3.2 Polarized Structure Functions in Inclusive Electron Scattering

The differential cross section for inclusive scattering of polarized electrons from polarized protons  $p(\vec{e}, e')X$  can be expressed in the following way:

$$\frac{d\sigma}{d\Omega_e dE'_e} =$$

$$\Gamma_T \cdot [\sigma_T + \epsilon\sigma_L + P_e \cdot P_p \cdot \cos\phi \cdot (\sqrt{1-\epsilon^2} \cdot \cos\psi \cdot A_1 \cdot \sigma_T + \sqrt{\epsilon(1-\epsilon)} \cdot \sin\psi \cdot A_2 \cdot \sigma_T)] \quad (8)$$

where  $\psi$  is the polar angle of the target polarization vector relative to the direction of the virtual photon,  $\phi$  is the corresponding azimuthal angle,  $P_e$  and  $P_p$  are the

electron and proton polarization, and

$$A_1 = \frac{\sigma_{1/2}^T - \sigma_{3/2}^T}{\sigma_{1/2}^T + \sigma_{3/2}^T}. \quad (9)$$

$A_2$  is a transverse-longitudinal interference term with an upper bound of

$$A_2 < \sqrt{\sigma_L/\sigma_T}. \quad (10)$$

Since  $\sigma_L/\sigma_T$  is small throughout the resonance region,  $A_2$  will remain relatively small too. The two polarization structure functions can be separated by polarizing the target in the scattering plane ( $\phi = 0$ ), and by varying the polarization angle  $\psi$  for fixed electron kinematics.

$A_1(W, Q^2)$  contains global information about the helicity structure of the nucleon resonances, and their dependences on  $Q^2$ . Comparisons with the behaviour of  $A_1$  in the deep inelastic regime should prove interesting. It is also needed as an ingredient for determining the  $Q^2$  evolution of the Gerasimov-Drell-Hearn sum rule (section 5). An experiment at SLAC measured a combination of  $A_1$  and  $A_2$  (Figure 3.5). Although the errors are large, an interesting  $Q^2$  dependence of the resonance was revealed; the helicity asymmetry in the region of  $W = 1.5 - 1.8 \text{ GeV}$ , showed a rapid change from helicity 3/2 dominance in photoproduction ( $Q^2 = 0$ ), to helicity 1/2 dominance at  $Q^2 = 0.5 \text{ GeV}^2$ . This "helicity switch" is in qualitative agreement with expectations from quark models for the prominent  $D_{13}(1520)$  and  $F_{15}(1680)$  resonances (see sections 4.3 and 4.4). The asymmetry in the mass region of the  $\Delta(1232)$  remained unchanged at  $\simeq -0.5$ , as expected from a dominant magnetic dipole transition. For pure  $M_{1+}$  transition one has  $\sigma_{1/2}/\sigma_{3/2} = 1/2$ . In the following section we illustrate the sensitivity of a measurement of  $A_1$  to the excitation strength of the Roper resonance  $P_{11}(1440)$ .

### 3.2.1 Sensitivity of $A_1$ to Roper Excitation

Since the Roper resonance  $P_{11}(1440)$ , has spin 1/2, it can only be excited by helicity 1/2 amplitudes ( $A_{1/2}$  or  $S_{1/2}$ ).  $A_1$  is sensitive to the strength of the resonance transition. For a strong  $P_{11}$  excitation the asymmetry  $A_1$  tends to be more positive than for a weak  $P_{11}$  excitation. Since for an isolated  $\Delta(1232)$  or  $P_{11}(1440)$ , the asymmetry is  $A_1 = -0.5$  or  $+1$ , respectively, and independent of  $Q^2$ , the relative strength of the Roper will strongly affect the actual asymmetry in the overlap region of the two states. Expected statistical error bars of an experiment proposed for CEBAF are shown in Figure 3.6.

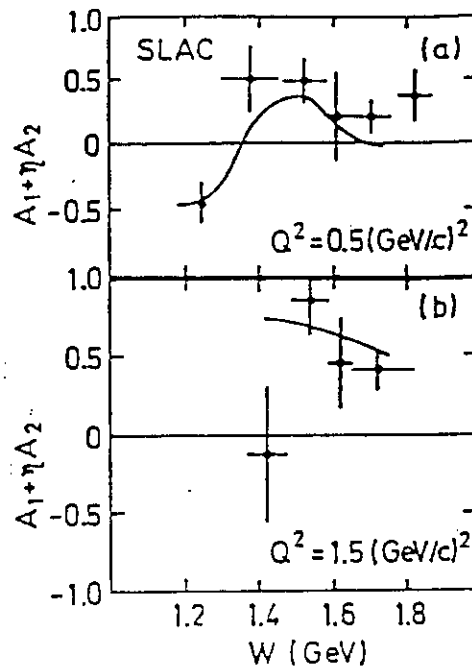


Figure 3.5 Polarized Inclusive Structure Function  $A_1 + \eta A_2$  as measured at SLAC<sup>30</sup>.

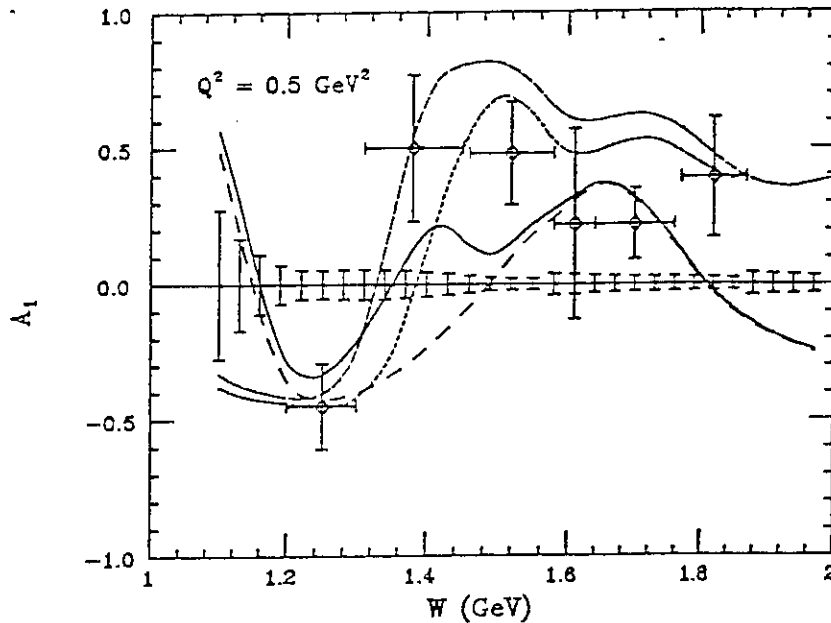


Figure 3.6 Polarized structure function  $A_1$  in the resonance region at fixed  $Q^2$ . The short dashed curves represent calculations based on the NRQM of Close and Li<sup>43</sup>, with different assumptions about the transition amplitudes of the Roper. The other curves are the result of a semi-empirical calculation<sup>71</sup> that fits the single pion production data. Same assumptions about the Roper amplitudes are used. The short error bars are expectations for an approved CEBAF experiment<sup>31</sup> that will cover  $0.25 < Q^2 < 2.0 \text{ GeV}^2$  and  $1.1 < W < 2.0 \text{ GeV}$ .

#### 4. EXCLUSIVE ELECTROPRODUCTION EXPERIMENTS

Inclusive measurements do not allow identification of the excited states. This can only be accomplished by explicit measurement of the decay products such as  $\pi N$ ,  $\eta N$ ,  $\rho N$ ,  $\pi\Delta$ . The  $\gamma_\nu NN^*$  vertex for the transition into a specific state is described by two (for  $J=1/2$  states) or three (for  $J \geq 3/2$  states) amplitudes,  $A_{1/2}(Q^2)$ ,  $A_{3/2}(Q^2)$ , and  $S_{1/2}(Q^2)$ , where A and S refer to the transverse and scalar coupling, respectively, and the subscripts refer to the total helicity of the  $\gamma_\nu N$  system (Figure 4.1). Spin and isospin can be extracted by measuring the angular distribution in different isospin channels. Many of the low lying resonances decay primarily into the  $N\pi$  or  $N\eta$  channels. Experiments have therefore concentrated on single  $\pi$  and  $\eta$  production. In the following section our current knowledge of the resonance transition amplitudes resulting from these reactions is reviewed. Detailed information and an exhaustive list of references are given in an excellent review article by Foster and Hughes<sup>32</sup>.

Very little is known about multiple pion production processes. Some global information about the reactions  $p(e, e' p\rho)$ ,  $p(e, e' \pi\Delta(1232))$  have been obtained from a DESY streamer chamber experiment<sup>33</sup>. However, the data are not sufficiently detailed to allow the extraction of helicity amplitudes for specific resonances.

##### 4.1 Multipoles and Partial Wave Helicity Elements.

The differential cross section in single meson production contains four response functions:

$$\frac{d\sigma}{d\Omega} = \sigma_T + \epsilon\sigma_L + \epsilon\sigma_{TT} \cos 2\phi + \sqrt{2\epsilon(1+\epsilon)}\sigma_{TL} \cos \phi \quad (11)$$

where  $\phi$  is the azimuthal angle of the hadronic decay plane with respect to the electron scattering plane. The observables of the process  $\gamma_\nu N \rightarrow \pi N$ , where  $\gamma_\nu$  denotes the virtual photon, can be expressed in term of parity conserving helicity amplitudes<sup>34</sup>:

$$H_i := \langle \lambda_\pi; \lambda_N | T | \lambda_{\gamma_\nu}; \lambda_p \rangle = \langle 0; \pm \frac{1}{2} | T | \pm 1, 0; \pm \frac{1}{2} \rangle \quad (12)$$

where  $\lambda$  denotes the helicity of the respective particle. The  $H_i$  are complex functions of  $Q^2$ ,  $W$ ,  $\theta_\pi^*$ . The response functions are given by:

$$\sigma_T = \frac{|\vec{p}_\pi|W}{2kM} \cdot (|H_1|^2 + |H_4|^2 + |H_5|^2 + |H_6|^2) \quad (13)$$

$$\sigma_L = \frac{|\vec{p}_\pi|W}{kM} \cdot (|H_5|^2 + |H_6|^2)$$

$$\sigma_{TT} = \frac{|\vec{p}_\pi|W}{kM} \cdot \text{Re}(H_2 H_3^* - H_1 H_4^*)$$

$$\sigma_{TL} = \frac{|\vec{p}_\pi|W}{\sqrt{2}kM} \cdot \text{Re}(H_5^*(H_1 - H_4) + H_6^*(H_2 + H_3))$$

where  $\vec{p}_\pi$  is the pion momentum in the hadronic cms system, and  $k$  is the equivalent real photon energy for producing a state with mass  $W$ :

$$k = \frac{W^2 - M^2}{2M}$$

The  $H_i$  can be expanded in terms of Legendre polynomials:

$$H_1 = \frac{1}{2} \sqrt{2} \sin \theta \cos \frac{\theta}{2} \sum_{l=1}^{\infty} (B_{l+} - B_{(l+1)-}) (P_l'' - P_{l+1}'')$$

$$H_2 = \sqrt{2} \cos \frac{\theta}{2} \sum_{l=0}^{\infty} (A_{l+} - A_{(l+1)-}) (P_l' - P_{l+1}')$$

$$H_3 = \frac{1}{2} \sqrt{2} \sin \theta \sin \frac{\theta}{2} \sum_{l=1}^{\infty} (B_{l+} + B_{(l+1)-}) (P_l'' + P_{l+1}'')$$

$$H_4 = \sqrt{2} \sin \frac{\theta}{2} \sum_{l=0}^{\infty} (A_{l+} + A_{(l+1)-}) (P_l' + P_{l+1}')$$

$$H_5 = \sqrt{2} \cos \frac{\theta}{2} \sum_{l=0}^{\infty} (C_{l+} - C_{(l+1)-}) (P_l' - P_{l+1}')$$

$$H_6 = \sqrt{2} \sin \frac{\theta}{2} \sum_{l=0}^{\infty} (C_{l+} + C_{(l+1)-}) (P_l' + P_{l+1}') \quad (14)$$

$A_{l\pm}$  and  $B_{l\pm}$  are the transverse partial wave helicity elements for  $\lambda_\gamma = \frac{1}{2}$  and  $\lambda_\gamma = \frac{3}{2}$ , respectively.  $C_{l\pm}$  are the longitudinal partial wave helicity elements. In the subscript  $l\pm$ ,  $l$  is the  $\pi$  ( $\eta$ ) orbital angular momentum, and  $\pm$  is related to the total angular momentum,  $J = l \pm \frac{1}{2}$ . The partial wave helicity elements are linear combinations of the electromagnetic multipoles  $M_{l\pm}$ ,  $E_{l\pm}$ ,  $S_{l\pm}$ :

$$M_{l+} = \frac{1}{2(l+1)} (2A_{l+} - (l+2)B_{l+})$$

$$E_{l+} = \frac{2}{(l+1)} (2A_{l+} + lB_{l+})$$

$$\begin{aligned}
M_{l+1,-} &= \frac{1}{l+1}(2A_{l+1,-} + lB_{l+1,-}) \\
E_{l+1,-} &= \frac{2}{l+1}(-2A_{l+1,-} + (l+2)B_{l+1,-}) \\
S_{l+} &= \frac{1}{l+1} \sqrt{\frac{\bar{Q}^{-2}}{Q^2}} C_{l+} \\
S_{l+1,-} &= -\frac{1}{l+1} \sqrt{\frac{\bar{Q}^{-2}}{Q^2}} C_{l+1,-}
\end{aligned} \tag{15}$$

$\bar{Q}$  is the photon 3-momentum in the hadronic rest frame. The partial wave helicity elements contain both non-resonant and resonant contributions. An analysis must be performed to separate off the resonant parts  $\hat{A}_{l\pm}$ ,  $\hat{B}_{l\pm}$ , and  $\hat{C}_{l\pm}$  of the amplitudes. A detailed discussion of analysis methods is given in an excellent article by Moorhouse<sup>70</sup>. In a final step the known hadronic properties of a given resonance can be used to determine the photocoupling helicity amplitudes which characterize the electromagnetic vertex:

$$\hat{A}_{l\pm} = \mp K \cdot C_{\pi N}^I \cdot A_{1/2} \tag{16}$$

$$\hat{B}_{l\pm} = \pm K \sqrt{\frac{16}{(2j-1)(2j+3)}} C_{\pi N}^I A_{3/2} \tag{17}$$

$$K = \sqrt{\frac{1}{(2j+1)\pi} \frac{k}{p_\pi} \frac{M}{W_R} \frac{\Gamma_\pi}{\Gamma^2}}$$

where the  $C_{\pi N}^I$  are isospin coefficients. The total absorption cross section for the transition into a specific resonance is given by:

$$\sigma_T = \frac{2M}{W_R \Gamma} (A_{1/2}^2 + A_{3/2}^2) \tag{18}$$

The  $A_{1/2}$  and  $A_{3/2}$  are the quantities usually used to connect theoretical calculations to the experimental analysis. However, some models such as the Skyrme model, make direct predictions for the partial wave helicity elements<sup>35</sup>.

## 4.2 Radiative Transitions with $\Delta L_{3Q} = 0$

### 4.2.1 The Transition $\gamma_\nu p \rightarrow \Delta^+(1232)$ .

In SU(6) symmetric quark models, this transition is explained by a simple quark spin-flip in the  $L_{3Q} = 0$  ground state, corresponding to a magnetic dipole

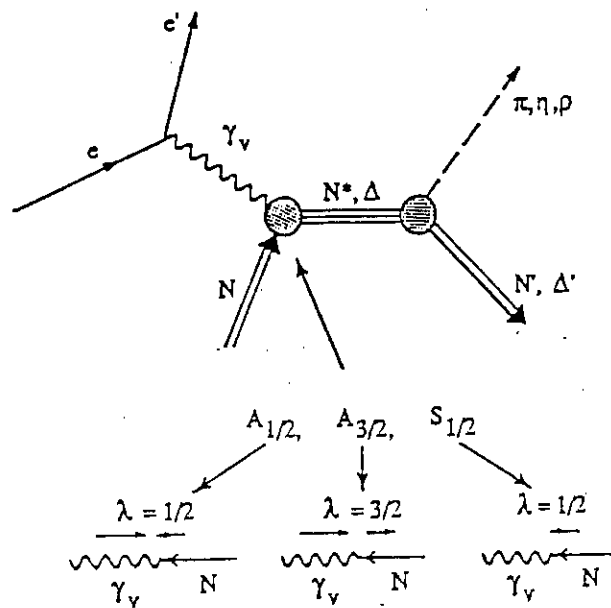


Figure 4.1 Electroproduction of hadronic final states via  $s$ -channel resonance decays. The  $\gamma_v NN^*$  vertex is described by the photocoupling helicity amplitudes  $A_{1/2}$ ,  $A_{3/2}$ , and  $S_{1/2}$ , which are functions of  $Q^2$  only.

transition  $M_{1+}$ . The electric and scalar quadrupole transitions are predicted to be  $E_{1+} = S_{1+} = 0$ . In more elaborate QCD based models which include color magnetic interactions arising from the one-gluon exchange at small distances, the  $\Delta(1232)$  acquires an  $L_{3Q} = 2$  component which leads to small electric and scalar contributions. Dynamical quark model calculations predict  $E_{1+}/M_{1+}$  to remain small ( $\leq 0.1$ ) in a large  $Q^2$  range.  $E_{1+}/M_{1+}$  is predicted to have a weak dependence on  $Q^2$ . At very high  $Q^2$ , helicity conservation requires<sup>24</sup>  $E_{1+}/M_{1+} \rightarrow 1$ , and  $S_{1+}/M_{1+} \rightarrow 0$ . Precise measurements of these contributions from  $Q^2 = 0$  to very large  $Q^2$  are obviously important for the development of realistic models of the nucleon.

In the region of the  $\Delta(1232)$ , one may expect that only  $s$ - and  $p$ -waves with  $J \leq 3/2$  contribute. If one further assumes dominance of the magnetic dipole transition and retains only terms in the cross section that contain the  $M_{1+}$  multipole, the cross section reduces to:

$$\begin{aligned}
\frac{d\sigma}{d\Omega} \simeq \frac{|\vec{E}_+|^2}{k} \cdot & \left[ \frac{3}{2}|M_{1+}|^2 - 3\text{Re}(M_{1+}E_{1+}^*) + \text{Re}(M_{1+}M_{1-}^*) \right. \\
& + 2\cos\theta\text{Re}(E_{0+}M_{1+}^*) \\
& + \cos^2\theta \left( -\frac{3}{2}|M_{1+}|^2 + 9\text{Re}(M_{1+}E_{1+}^*) - 3\text{Re}(M_{1-}M_{1+}^*) \right) \\
& + \epsilon\sin^2\theta\cos 2\phi \left( -\frac{3}{2}|M_{1+}|^2 - 3\text{Re}(M_{1+}E_{1+}^*) \right) \\
& \left. - \sqrt{2\epsilon_L(\epsilon+1)}\sin\theta\cos\phi \left( \text{Re}(S_{0+}M_{1+}^*) + 6\cos\theta\text{Re}(S_{1+}M_{1+}^*) \right) \right] \quad (19)
\end{aligned}$$

where  $\theta$  is the pion cms polar angle, and  $\epsilon_L = Q^2/(\vec{Q}^*)^2\epsilon$ . The sensitivity to the electric and scalar quadrupole transitions lies in the interference terms of  $E_{1+}$  and  $S_{1+}$  with  $M_{1+}$ .

In this approximation the resonant terms

$$|M_{1+}|, \text{Re}(M_{1+}E_{1+}^*), \text{Re}(M_{1+}S_{1+}^*)$$

and the non-resonant terms

$$\text{Re}(E_{0+}M_{1+}^*), \text{Re}(S_{0+}M_{1+}^*), \text{and } \text{Re}(M_{1-}M_{1+}^*)$$

can be determined uniquely by measuring the  $\phi$  and  $\theta$  dependence of the differential cross section.

Present experimental information about  $\text{Re}(E_{1+}M_{1+}^*)/|M_{1+}|^2$  at the  $\Delta(1232)$  resonance mass is shown in Figure 4.2. The quality of the data is clearly not sufficient to discriminate against any of the models.

Experiments at MIT-Bates<sup>37</sup> and CEBAF<sup>38</sup> are in preparation to measure the electric and scalar quadrupole transition over a large  $Q^2$  range, using polarized electron beams and/or recoil polarimeters. In these experiments one obtains information not only about the terms

$$M_{1+}, \text{Re}(E_{1+}M_{1+}^*), \text{Re}(S_{1+}M_{1+}^*)$$

but also about the corresponding imaginary parts:

$$\text{Im}(E_{1+}M_{1+}^*), \text{Im}(S_{1+}M_{1+}^*).$$

The imaginary parts of the bilinear terms can be measured only by using polarization degrees of freedom. They are particularly sensitive to phase relations between

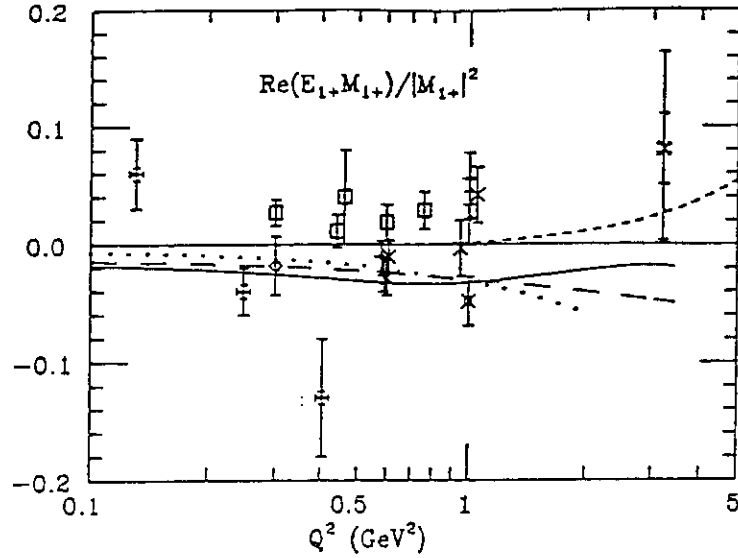


Figure 4.2 Ratio  $E_{1+}/M_{1+}$  from electroproduction experiments<sup>36</sup>

the multipoles. If the multipoles were strictly in phase, these terms would vanish identically.

#### 4.2.2 The Transition $\gamma_n p \rightarrow P_{11}^+(1440)$ .

The Roper resonance is often characterized as a “breathing” mode or a radial excitation of the nucleon. Electromagnetic excitation of the Roper resonance  $P_{11}(1440)$  is of particular interest as one can test the spectroscopic assignment of this state by measuring the transition form factors. Difficulties in describing its radiative decay width with quark models have prompted speculations<sup>39</sup> about the nature of the  $P_{11}(1440)$ . The SU(6) classification of the  $P_{11}(1440)$  is that of a  $[56, 0^+]_2$  state. The non-relativistic quark model predicts for the neutron/proton ratio:  $A_{1/2}^n/A_{1/2}^p = -2/3$ , whereas a relativized quark model<sup>39</sup> gives a much smaller value. In chiral bag model calculations<sup>40</sup> contributions from the pion cloud of the proton bring this ratio closer to -1 at  $Q^2 = 0$ . With increasing  $Q^2$ , however, the role of the pion cloud should be diminished, and the quark composition is expected to dominate the excitation of the Roper at higher  $Q^2$ . Precise data on photo- and electroexcitation of the Roper can help reveal the true nature of this state. An interesting consequence of the  $N = 2$  assignment of the  $P_{11}(1440)$  within the framework of the NRQM is its predicted dominance over the  $\Delta(1232)$  at high  $Q^2$ . The NRQM predicts<sup>41</sup>:

$$\frac{A_{1/2}(P_{11}(1440))}{A_{1/2}(P_{33}(1232))} \propto \bar{Q}^2 \quad (20)$$

The data are shown in Figure 4.3. The value -2/3 is clearly preferred for the neu-

tron/proton ratio, although a value closer to -1 is not ruled out. The  $Q^2$  dependence is not known very well and none of the explicit quark models comes even near to describing both the photon point and the  $Q^2$  behaviour suggested by the data. Relativistic corrections give uncomfortably large effects, casting some doubt on the reliability of the calculations. Predictions for the longitudinal (scalar) coupling appear to be less sensitive to relativistic corrections. The transition to the  $P_{11}(1440)$  is predicted to exhibit an exceptionally strong longitudinal coupling, a feature which is not supported by the data.  $S_{1/2}$  is consistent with a small value, or even zero, although significant values at small  $Q^2$  cannot be excluded. Clearly, more precise and more complete data are needed to study the apparently strong  $Q^2$  dependence at small  $Q^2$ .

### 4.3 Radiative Transitions between the $[56, 0^+]_0$ and the $[70, 1^-]_1$ Multiplets

Of the seven non-strange states associated with the  $[70, 1^-]_1$  multiplet only the  $D_{13}(1520)$  and the  $S_{11}(1535)$  have been studied in electroproduction experiments in some detail.

#### 4.3.1 The $\gamma_{\nu p} \rightarrow S_{11}(1535)$ Transition

The  $S_{11}(1535)$  is characterized by a large branching ratio into the  $\eta N$  channel ( $\approx 50\%$ ). Since the nearby  $D_{13}(1520)$  state has a very small decay width into  $\eta N$  the  $S_{11}(1535)$  can be separated off in a rather straight forward manner<sup>67,68</sup>. Electroproduction results indicate a very slow falloff with  $Q^2$  (Figure 4.4). Up until recently, this behavior could not be explained within the framework of quark models. However, recent extensions of the model to include relativistic effects have been quite successful in reproducing this particular behavior. It is interesting to note that within the framework of a specific model, the absolute normalization and the  $Q^2$  dependence appear to be sensitive to the parameterization of the confinement potential. This lends confidence to the idea that a great deal can be learned about the properties of the confinement potential by carefully studying many resonance transitions.

#### 4.3.2 The $\gamma_{\nu p} \rightarrow D_{13}(1520)$ Transition

At  $Q^2 = 0$ , the  $D_{13}(1520)$  is predominantly excited by  $A_{3/2}$  transitions. With increasing  $Q^2$ ,  $A_{1/2}$  becomes the dominant contribution. This is demonstrated by displaying the helicity asymmetry

$$A_{\frac{1}{2}, \frac{3}{2}} = \frac{A_{1/2}^2 - A_{3/2}^2}{A_{1/2}^2 + A_{3/2}^2} \quad (21)$$

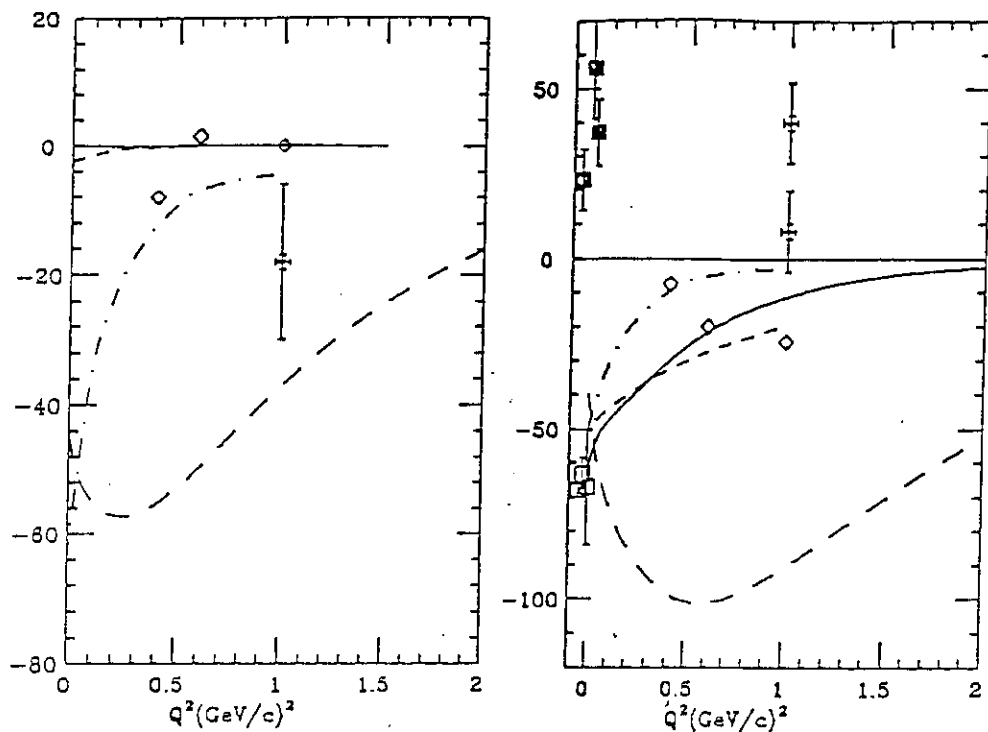


Figure 4.3 Transverse (left) and scalar (right) photocoupling amplitudes of the Roper  $P_{11}(1440)$  for proton (open symbols) and neutron (full squares) targets. The open diamond symbols and the short dashed and dashed-dotted lines represent results of a fixed- $t$  dispersion relation fit by Gerhardt<sup>66</sup>. Long dashes represent calculations for protons within the NRQM with QCD mixing of Close and Li<sup>43</sup>. The solid lines are the result of a calculation assuming the Roper is a gluonic excitation of the nucleon (See section (5.1)). Only calculations that approximately reproduce the photon point have been included.

A summary of the data is presented in Figure 4.5. It is worth noting that effects due to the spatial wave function tend to cancel out in this quantity. The helicity asymmetry is therefore sensitive to the spin-flavor wavefunction. The helicity switch agrees qualitatively with quark model predictions<sup>46</sup>, as well as with expectations from helicity conservation in perturbative QCD at high  $Q^2$ . However, the details, of how, and at what  $Q^2$  this transition occurs will provide us with more insight into the internal dynamics of the nucleon<sup>39</sup>.

#### 4.3.3. Test of the Single Quark Transition Model

Within the framework of single quark transitions in  $SU(6)_W$  symmetric models, radiative transitions between the  $[56, 0^+]_0$  and the  $[70, 1^-]_1$  multiplet are described by 3 amplitudes<sup>47</sup>, often called A, B, and C, where A is related to the quark orbit

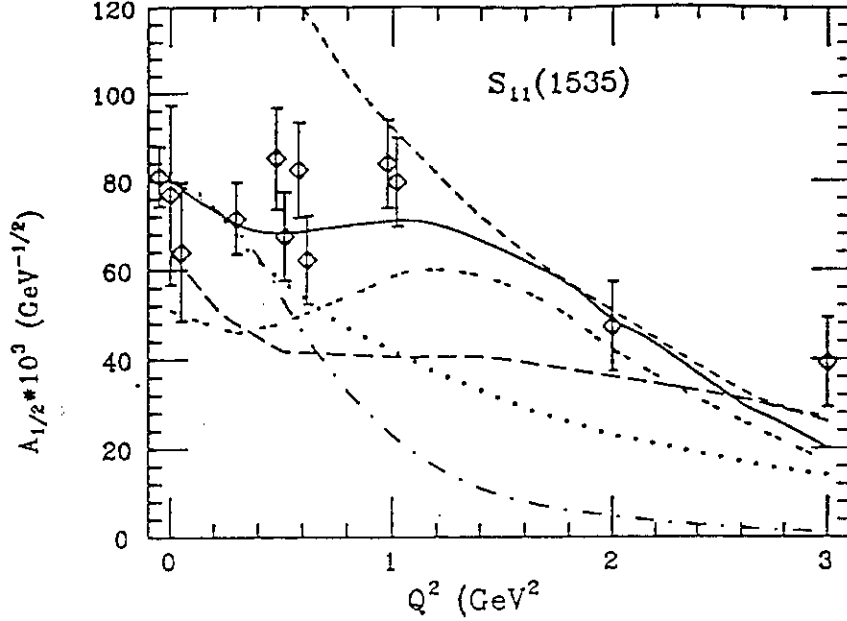


Figure 4.4 Transverse amplitude  $A_{1/2}$  for the transition  $\gamma_p S_{11}(1535)$ . Model calculations by Close and Li<sup>43</sup> (short dashes), Warns et al<sup>29</sup> (solid line, double-dashed line for different confinement potentials), Foster and Hughes<sup>42</sup> (dots), Konen and Weber<sup>44</sup> (long dashes), Forsyth and Babcock<sup>45</sup> (dashed-dotted).

flip current, B to the quark spin flip current, and C to the combined spin flip and orbit flip current with  $\Delta L_z = 1$ , respectively. In the framework of the single quark transition model (SQTm) radiative transitions between all states belonging to these multiplets can be expressed in terms of linear combinations of these amplitudes (table 4.1).

Knowledge of the  $A_{1/2}$ ,  $A_{3/2}$  amplitudes for the  $S_{11}(1535)$  and the  $D_{13}(1520)$  states allows one to determine the A, B, C single quark transition amplitudes. These can then be used to predict transition amplitudes for other states. Recoil effects may generate deviations from the SQTm at the 20% level<sup>29</sup>. Unfortunately, information from other states is limited to proton targets and is of poor quality. Current experimental information of the  $S_{11}(1650)$ ,  $S_{31}(1620)$ , and  $D_{33}(1700)$  is summarized in Figure 4.6. The data are not in disagreement with the SQTm predictions, but they are not accurate enough to test deviations from the SQTm at the predicted level.

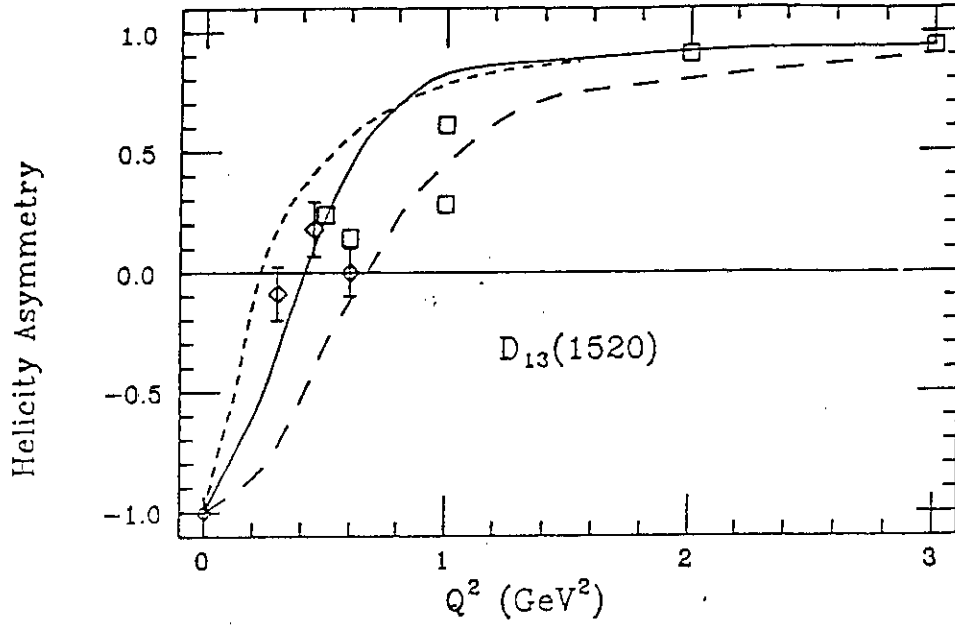


Figure 4.5 Helicity asymmetry of the  $\gamma_v p D_{13}(1520)$  transition. Quark-model calculations by Ono<sup>48</sup> (long dashes), Copley et al.<sup>41</sup> (short dashes), Close and Li<sup>43</sup> (NRQM with QCD mixing, solid).

#### 4.3.4 Quark Multipoles for $\gamma_v + [56, 0^+]_0 \rightarrow [70, 1^-]_1$

The single quark transition amplitudes can be expressed in terms of quark electric and quark magnetic multipoles<sup>49</sup>,  $e_\lambda^{LL}$ ,  $m_\lambda^{LL}$ ,  $m_\lambda^{L,L+1}$ , which are related to the quark orbit flip, the quark spin flip, and the quark spin-orbit flip amplitudes, respectively. For the transition  $[56, 0^+]_0 \rightarrow [70, 1^-]_1$  one obtains<sup>50</sup> (in units of  $[\mu b GeV]^{1/2}$ ):

$$\begin{aligned}
 A &= 8.88 e_1^{11} \\
 1/2(B - C) &= -6.31 m_1^{11} \\
 1/2(B + C) &= +6.31 m_1^{12}
 \end{aligned} \tag{22}$$

More direct information about the photon quark dynamics can be obtained by factoring out an explicit dipole form factor dependence

$$F(\bar{Q}_{evf}^2) = \frac{1}{(1 + \bar{Q}_{evf}^2/0.71)^2},$$

Table 4.1 Single Quark Transition Amplitudes for  $\gamma + [56, 0^+]_0 \rightarrow [70, 1^-]_1$ 

State	Proton Target	Neutron Target
$S_{11}(1535)$ :	$A_{\frac{1}{2}}^+ = \frac{1}{6}(A + B - C)\cos\theta^+$	$A_{\frac{1}{2}}^0 = -\frac{1}{6}(A + \frac{1}{3}B - \frac{1}{3}C)$
$D_{13}(1520)$ :	$A_{\frac{1}{2}}^+ = \frac{1}{6\sqrt{2}}(A - 2B - C),$ $A_{\frac{3}{2}}^+ = \frac{1}{2\sqrt{6}}(A + C)$	$A_{\frac{1}{2}}^0 = -\frac{1}{18\sqrt{2}}(3A - 2B - C)$ $A_{\frac{3}{2}}^0 = \frac{1}{6\sqrt{6}}(3A - C)$
$S_{11}(1650)$ :	$A_{\frac{1}{2}}^+ = \frac{1}{6}(A + B - C)\sin\theta$	$A_{\frac{1}{2}}^0 = \frac{1}{18}(B - C)$
$D_{13}(1700)$ :	$A_{\frac{1}{2}}^+ = A_{\frac{3}{2}}^+ = 0^{++}$	$A_{\frac{1}{2}}^0 = \frac{1}{18\sqrt{5}}(B - 4C)$ $A_{\frac{3}{2}}^0 = \frac{1}{6\sqrt{15}}(3B - 2C)$
$D_{15}(1670)$ :	$A_{\frac{1}{2}}^+ = A_{\frac{3}{2}}^+ = 0^{++}$	$A_{\frac{1}{2}}^0 = -\frac{1}{6\sqrt{5}}(B + C)$ $A_{\frac{3}{2}}^0 = \frac{1}{6}\sqrt{\frac{2}{5}}(B + C)$
$D_{33}(1670)$ :	$A_{\frac{1}{2}}^+ = \frac{1}{18\sqrt{2}}(3A + 2B + C)$ $A_{\frac{3}{2}}^+ = \frac{1}{6\sqrt{5}}(3A - C)$	same same
$S_{31}(1650)$ :	$A_{\frac{1}{2}}^+ = \frac{1}{3}(3A - B + C)$	same

$+$  ( $\theta$  = mixing angle between  ${}^4[8]_{1/2}$  and  ${}^2[8]_{1/2}$  in  $\{70, 1^-\}_1$ )

$++$  unless mixed with states in other supermultiplets

where the 3-momentum is evaluated in the equal velocity frame ( $\vec{v}_N = -\vec{v}_N$ ) to minimize relativistic effects. The only justification for such a choice is that it describes the  $Q^2$  dependence of the elastic formfactor (note that  $\bar{Q}_{evf}^2 = Q^2$  for elastic scattering). Using this expression one can define reduced quark multipoles:

$$\begin{aligned}
 e_1^{11} &= \bar{e}_1^{11} F(\bar{Q}_{evf}^2); \quad m_1^{11} = \bar{m}_1^{11} F(\bar{Q}_{evf}^2); \\
 m_1^{12} &= \bar{m}_1^{12} F(\bar{Q}_{evf}^2) \\
 e_1^{22} &= \bar{e}_1^{22} |\bar{Q}_{evf}| F(\bar{Q}_{evf}^2); \quad m_1^{22} = \bar{m}_1^{22} |\bar{Q}_{evf}| F(\bar{Q}_{evf}^2); \\
 m_1^{23} &= \bar{m}_1^{23} |\bar{Q}_{evf}| F(\bar{Q}_{evf}^2)
 \end{aligned} \tag{23}$$

The results for the  $[70, 1^-]_1$  multiplet are displayed in Figure 4.7. The reduced multipoles  $\bar{e}_1^{11}$ , and  $\bar{m}_1^{11}$  exhibit a very simple  $\bar{Q}_{evf}^2$  dependence.  $\bar{e}_1^{11}$  is independent

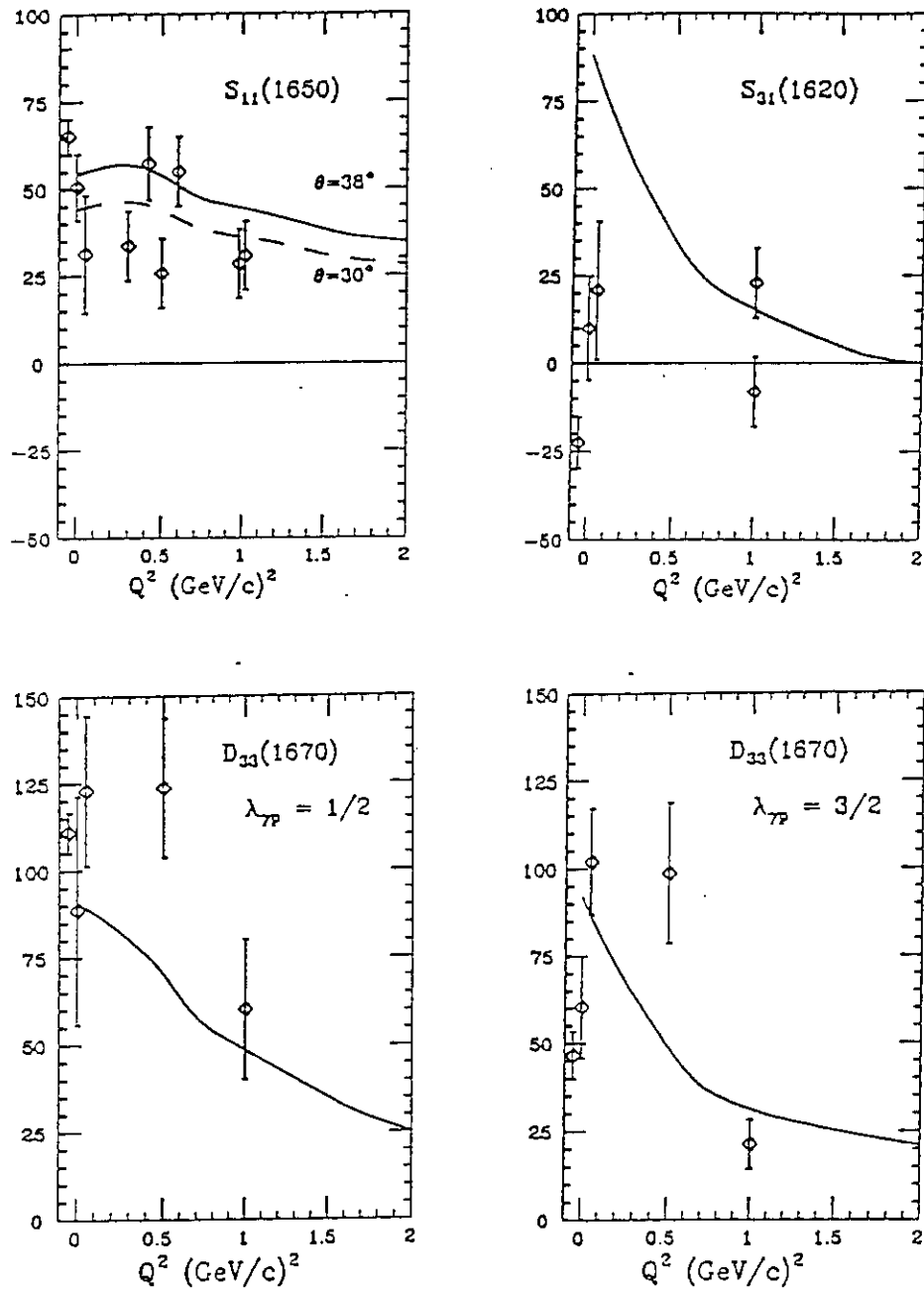


Figure 4.6 Transverse photocoupling amplitudes for the the  $S_{11}(1650)$ ,  $S_{31}(1620)$ , and  $D_{33}(1700)$  states. The curves represent SQTМ predictions using  $S_{11}(1535)$  and  $D_{13}(1520)$  data and the algebraic relations of Hey and Weyers<sup>47</sup>.  $\theta$  is the mixing angle between the  $[^48]$  and  $[^28]$  states in  $[70, 1^-]$ .

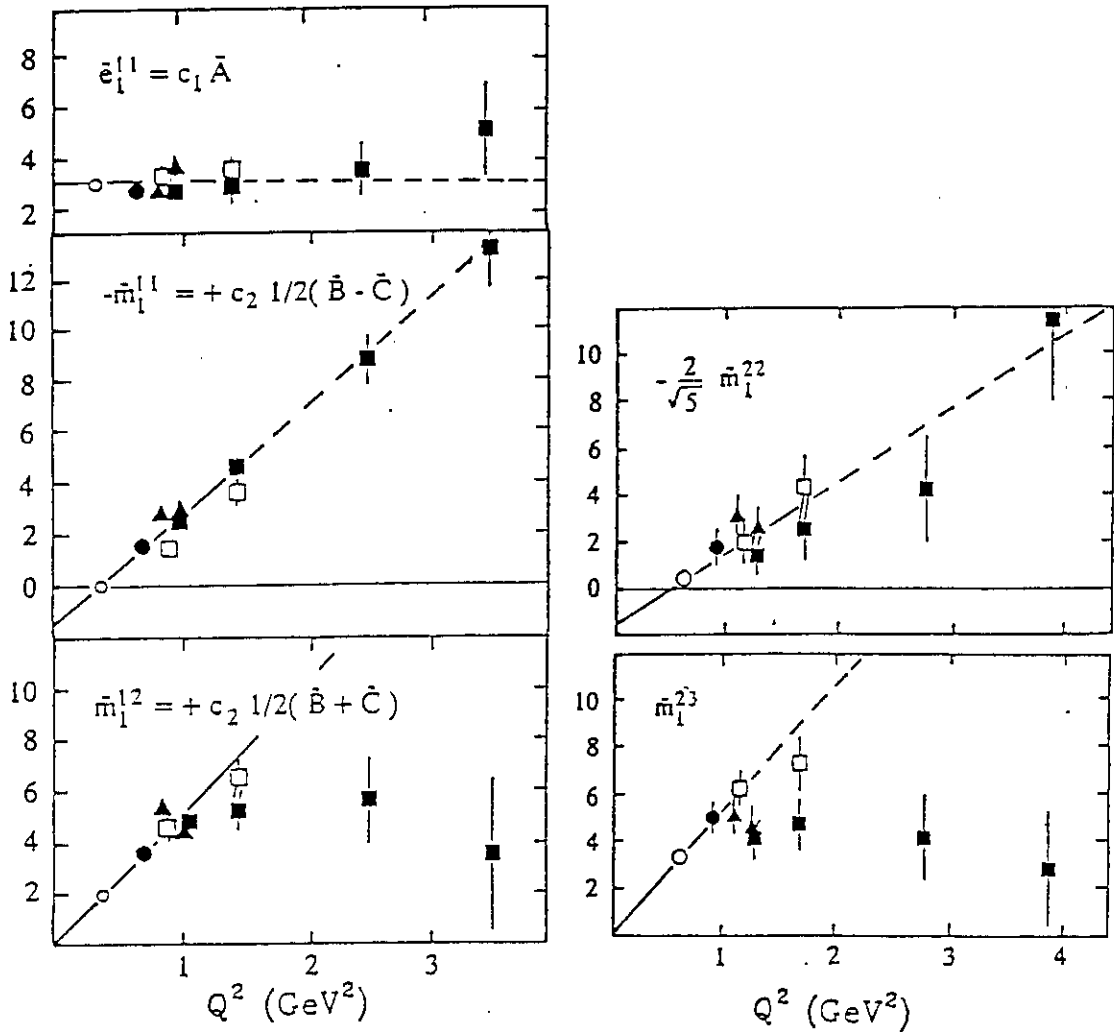


Figure 4.7 Reduced quark multipoles in units of [GeV] for the transition  $\gamma_v + [56, 0^+]_0 \rightarrow [70, 1^-]_1$  (left), and  $\gamma_v + [56, 0^+]_0 \rightarrow [56, 2^+]_2$  (right). For the transition to  $[56, 2^+]_2$  the orbit flip term has been assumed constant with the value  $\bar{e}_1^{22}$  determined at the photon point. The lines indicate the low  $\bar{Q}_{EVF}$  behavior.

of  $\bar{Q}_{evf}^2$ , and  $\bar{m}_1^{11}$  rises linearly with  $\bar{Q}_{evf}^2$ . At small  $\bar{Q}_{evf}^2$ ,  $\bar{m}_1^{12}$  has nearly the same slope as  $\bar{m}_1^{11}$ . This indicates that the reduced spin orbit term  $C$  is approximately constant at  $\bar{Q}_{evf}^2 < 1.5 \text{ GeV}^2$ . The simplicity of the  $\bar{Q}_{evf}^2$  dependence calls for a simple explanation. The simple non relativistic quark model (NRQM) provides an explanation of the reduced quark electric multipole being constant, and predicts

a linear rise of the reduced spin flip amplitude  $B$ , but since  $C = 0$ , the NRQM predicts  $m_1^{11} = m_1^{12}$ , in contrast to the experimental findings. The conclusion from these studies is that the electromagnetic current operator in the simple NRQM is not complete and has to be modified to include the spin-orbit transition term  $C$ .

#### 4.4 The Transition $\gamma_e + [56, 0^+]_0 \rightarrow [56, 2^+]_2$

The most prominent state of the  $[56, 2^+]_2$  super multiplet is the  $F_{15}(1688)$ , and it is the only one that has been studied experimentally over an extended  $Q^2$  range. Similar to the  $D_{13}^+(1520)$ , the photoexcitation is dominantly helicity 3/2 and hence  $A_{1/2}^+(F_{15}) \approx 0$ , at  $Q^2 = 0$ . The data show a rapid change in the helicity structure with rising  $Q^2$  (Figure 4.8). The switch to helicity 1/2 dominance is qualitatively reproduced by quark model calculations. However, much improved data are needed for a more definite comparison with the theory.

Without additional assumptions the four contributing SQTMs amplitudes  $A'$ ,  $B'$ ,  $C'$ , and  $D'$  (note that there is also a spin-orbit flip amplitude  $D'$  with  $\Delta L_z = 2$ ) presently can not be determined due to the lack of electroproduction data for a second state in the  $[56, 2^+]_2$  super multiplet. However, if we assume that the orbit flip term  $\bar{e}_1^{22}$  for this transition is independent of  $Q^2$  as it is for the  $[70, 1^-]_1$ , we can use the photoproduction value for  $\bar{e}_1^{22}$  and determine the reduced magnetic quark multipoles  $\bar{m}_1^{22}$  and  $\bar{m}_1^{23}$ . The results are shown in Figure 4.7.  $\bar{m}_1^{22}$  shows an approximately linear dependence on  $Q^2$ , similar to  $\bar{m}_1^{11}$ . The shift between  $-\frac{2}{\sqrt{3}}\bar{m}_1^{22}$  and  $\bar{m}_1^{23}$  indicates that there are significant contributions from  $C'$  and/or  $D'$ . This confirms the conclusion from the previous section that the simple electromagnetic current operator which acts only on the quark orbit and the spin is not complete. In fact, the discrepancy appears to increase with increasing  $Q^2$ .

## 5. NEW AND OLD PHYSICS TOPICS.

In this section I want to discuss some problems that have generated a great deal of interest in recent years. Their resolution may have a significant impact on our understanding of the baryon structure. These issues have either not been addressed, or have not been sufficiently addressed in previous experimental efforts.

### 5.1 Gluonic Excitations of Baryons States

Recently, there have been speculations about the existence of hybrid baryon states<sup>18,19</sup> consisting of 3 valence quarks and one valence gluon. The valence gluon

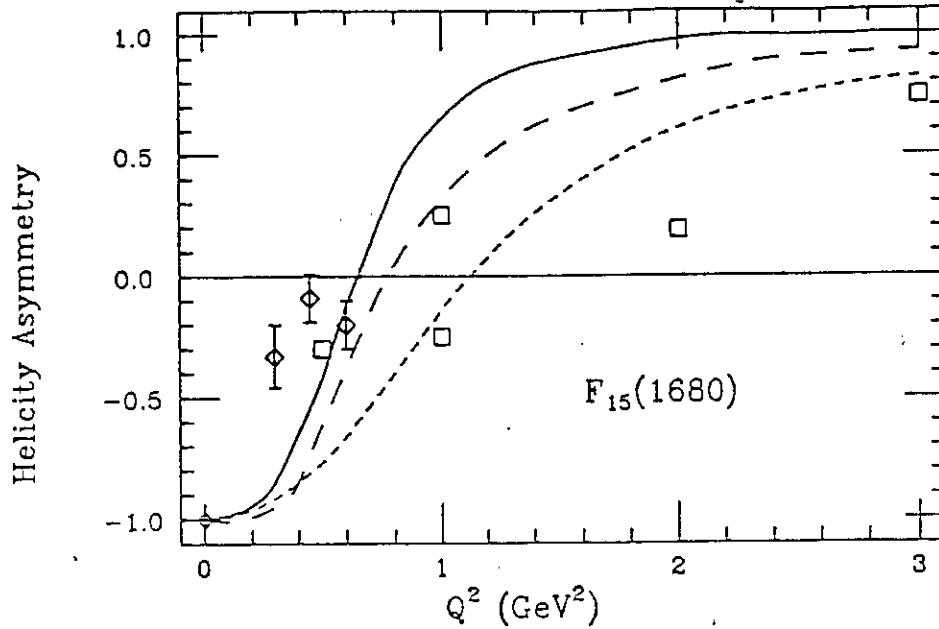


Figure 4.8 Helicity asymmetry for the  $\gamma_{\nu p} F_{15}(1680)$ . Same models as in Figure 4.5.

may give rise to additional baryonic states (gluonic excitations or hybrid states) that are denoted  $q^3 G$ . In hadronic production experiments these states cannot be distinguished from ordinary  $q^3$  states because they are, unlike hybrid mesons, characterized by quantum numbers which are also possible for the normal baryon states. The electromagnetic probe will be a powerful tool in these studies as it allows us to probe the different internal structure for  $q^3$  and  $q^3 G$  states.

#### 5.1.1 The $Q^2$ Quenching of the Roper $P_{11}(1440)$

The Roper has been discussed as a candidate for the lightest hybrid baryon<sup>21,22</sup>. If this were indeed the case, a long-standing problem in baryon structure, the strong quenching of the transition formfactor  $\gamma_{\nu p} P_{11}(1440)$  with  $Q^2$  could be resolved. In the following section I will discuss this aspect in some detail.

In the NRQM the lowest mass  $P_{11}(1440)$  state is assigned to a radially excited  $q^3$  state within the  $SU(6) \times O(3)$  super-multiplet  $[56, 0^+]_2$  (i.e.  $L_{3Q} = 0$ ,  $N_{3Q} = 2$ ). However, the observed low mass of the state, as well as the sign and magnitude of the photocoupling amplitudes have traditionally been difficult to reproduce within the framework of the NRQM. Moreover, as we have seen in section (4.2.2) there

is experimental evidence that the  $Q^2$  dependence of the photocoupling amplitude  $A_{1/2}(Q^2)$  is quite different from what is predicted in the framework of the NRQM. The data indicate a rapid fall-off of this amplitude with  $Q^2$  whereas the NRQM, as well as the relativized versions, predict a much weaker fall-off or even a rise with  $Q^2$ . However, the experimental information about electroproduction amplitudes of the Roper is rather limited, largely due to the complete lack of polarization data, and definite conclusions about the nature of the Roper cannot be drawn from existing data.

If the Roper is a  $q^3G$  state, then, because the gluon carries spin the longitudinal coupling is absent in lowest order.

Obviously, the solution of the puzzle concerning the correct assignment of the  $P_{11}(1440)$  could have enormous impact on our understanding of baryon structure and the dynamics of the strong interaction in the non-perturbative regime. How can we experimentally discriminate between these alternatives?

In a constituent quark and gluon picture a graph that is expected to contribute to gluonic excitations is the QCD Compton process  $\gamma q \rightarrow Gq$  (Figure 5.1)

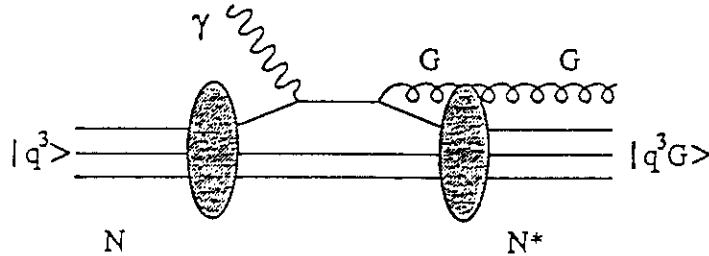


Figure 5.1 QCD Compton process in gluonic excitation

The inverse process  $Gq \rightarrow \gamma q$  has been studied in detail in hard scattering processes<sup>51</sup> and is well described in perturbative QCD.

A precise measurement of the  $Q^2$  dependence of the  $\gamma, p P_{11}(1440)$  transition form factor discriminates between the interpretation of the Roper as a regular  $[56, 0^+]_2 q^3$  state, or as a hybrid  $[70, 0^+]_0 q^3G$  state<sup>22</sup>. The discriminating power is a result of the fact that the respective photocoupling amplitudes are associated with different spin flavor factors, so that in the first approximation (if effects from the spatial wavefunction and relativistic corrections are neglected):

$$\frac{A_{1/2}(P_{11}(1440))[70, 0^+]_0}{A_{1/2}(P_{11}(1440))[56, 0^+]_2} \sim \frac{1}{Q^2} \quad (24)$$

Moreover, a composite system with four constituents will spatially be more extended than one with only three constituents, causing the form factor to drop even more quickly with  $Q^2$ . Therefore, accurate measurement of the  $Q^2$  dependence of the Roper photocoupling amplitude can be used to discriminate between these spectroscopic assignments. The calculation based on the hybrid interpretation is in better agreement with the data than calculations using the non-relativistic or relativized versions of the constituent quark model (Figure 4.3). However, it is possible that  $q^3$  models with strong mixing between the Roper and the ground state nucleon may be able to reproduce this fast drop with  $Q^2$ .

Very significant improvements in the quantity and statistical accuracy of the data base are expected from the experiments of the  $N^*$  collaboration at CEBAF<sup>38</sup>.

## 5.2 Missing $q^3$ Baryon States

The QCD motivated extensions of conventional quark models predict many states, with masses above 1.8, which have not been observed in  $\pi N \rightarrow \pi N$  reactions. Theoretical calculations<sup>14</sup> indicate that many of the "missing" states tend to decouple from the  $\pi N$  channel due to mixing, however, they may couple strongly to channels like  $\rho N$ ,  $\omega N$ , or  $\Delta\pi$ . It is experimentally well established that single pion production decreases with energy, while multi-pion production and vector meson production processes become more important (Figure 5.2). Electromagnetic production of these channels may therefore be the only way to study the "missing" states. In fact, several of those in the  $[56, 2^+]_2$  super multiplet are predicted to couple strongly to photons. For example, the  $F_{15}(1955)$ , and the  $F_{35}(1975)$  should be excited almost as strongly as some of the prominent states at lower masses. Search for these states is important and urgent. There are models, such as the quark cluster model<sup>16</sup> that can accommodate known baryon states, while predicting a few number of unobserved states. Experiments at CEBAF<sup>52</sup> and ELSA<sup>53</sup> to study electroproduction and photoproduction of vector mesons are expected to provide a definite answer for the existence of at least some of these states.

## 5.3 Baryon Resonance Transitions at High $Q^2$

At high energies, perturbative QCD makes simple predictions about the asymptotic  $Q^2$  behavior of the helicity amplitudes for resonance excitation. Based on the model of Brodsky and Lepage<sup>54</sup>, who factorize the process into a hard scattering part and a 'soft' non-perturbative part described by quark distribution functions, it is

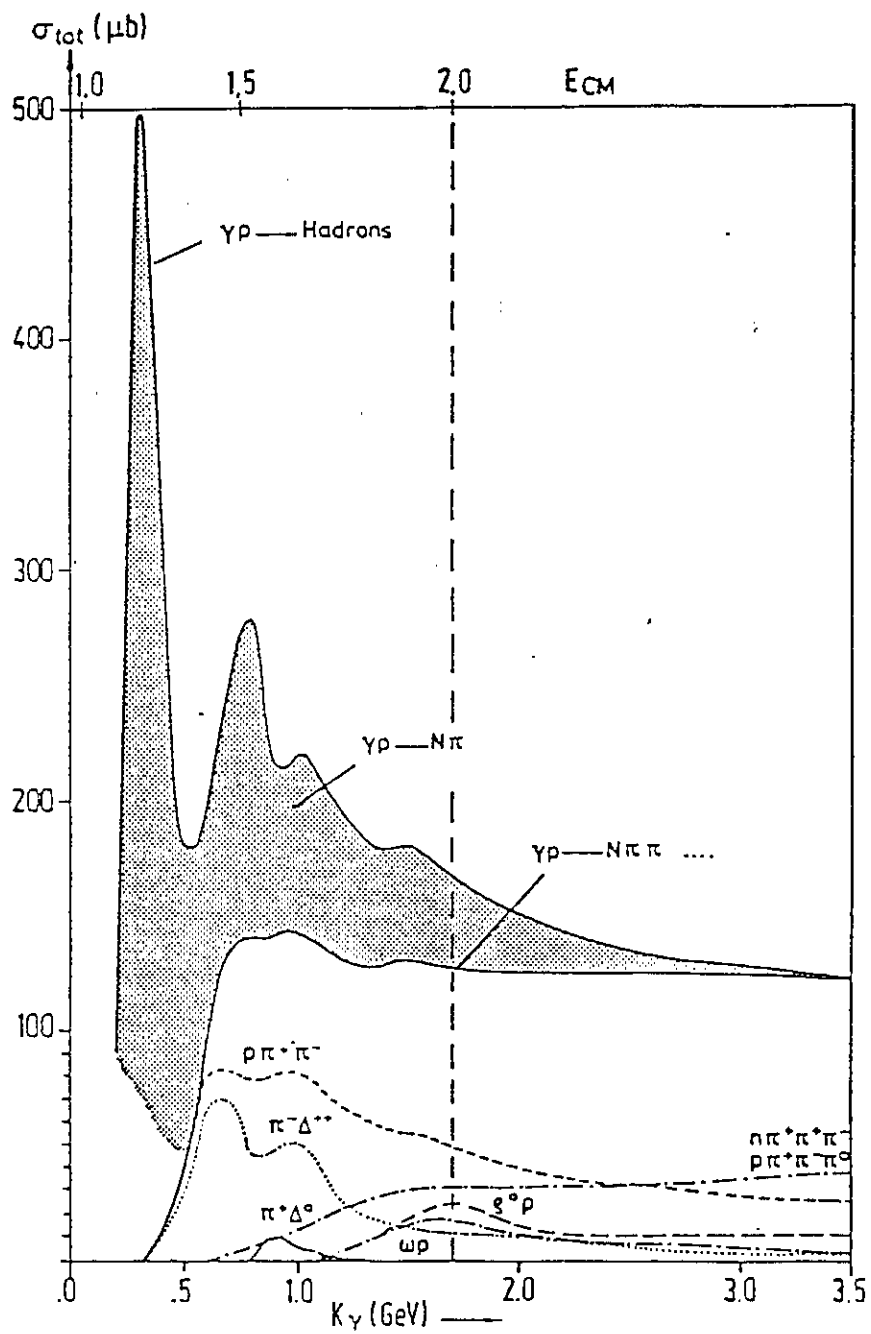


Figure 5.2 Photoabsorption and total photoproduction cross section for various exclusive channels.

expected<sup>24</sup> that

$$A_{1/2}(Q^2) = C_1/Q^3, \quad A_{3/2}(Q^2) = C_2/Q^5, \quad Q^2 \rightarrow \infty \quad (25)$$

if logarithmic terms are neglected. Information about the quark distribution functions and the normalization constant  $C_1$  can be obtained from QCD sum rules.

Of course, the first question to address is: At what momentum transfer does this description apply? Some interpretations<sup>24,25</sup> of the inclusive data have induced that the asymptotic behavior already is observed at  $Q^2 \approx 4$  to  $5 \text{ GeV}^2$ . However, others<sup>55</sup> have argued that asymptotic behavior will occur only at much higher  $Q^2$ . Conclusive tests require exclusive data, where the resonances are uniquely identified, and their respective helicity amplitudes have been separated. Separated data exist for  $Q^2 \leq 3 \text{ GeV}^2$  only, and only for a few states. In Figure 5.3 the  $A_{1/2}$  data are shown, multiplied by  $Q^3$ . The onset of the asymptotic regime would be indicated by the  $Q^2$  independence of this quantity. This is obviously not the case for this limited  $Q^2$  regime. However, it is interesting to note that at the highest  $Q^2$  the data are in the ballpark of the asymptotic predictions. It is also interesting to note that for the  $S_{11}(1535)$ , the calculations within the framework of relativized quark models, yield values for the highest  $Q^2$  point which are in the same ballpark as the asymptotic predictions. The non-relativistic version clearly fails for  $Q^2 > 0.6 \text{ GeV}^2$ .

#### 5.4 Multiple Quark Transitions

It is well known<sup>56</sup> that  $q^3$  baryon states belonging to the  $[20, 1^+]$  super multiplet with its antisymmetric wave function cannot be excited from the ground state in a single quark transition. The search for direct electromagnetic excitation of these states would allow a test of the SQT hypothesis. Calculations within the framework of a relativized quark model<sup>29</sup> indicate that multi quark transition (MQT) amplitudes may contribute at a level of 10 to 20% of those for SQT amplitudes of some of the prominent states. Clearly, the observation of these transitions requires high statistics measurements under conditions where interferences of the MQT amplitudes with other dominant amplitudes are important.

#### 5.5 $Q^2$ Evolution of the Gerasimov-Drell-Hearn Sum Rule

The results of the polarized proton structure function measurement of the EMC collaboration have prompted numerous speculations about whether or not in the deep inelastic region the spin of the proton is carried by the quarks<sup>57</sup>. This has

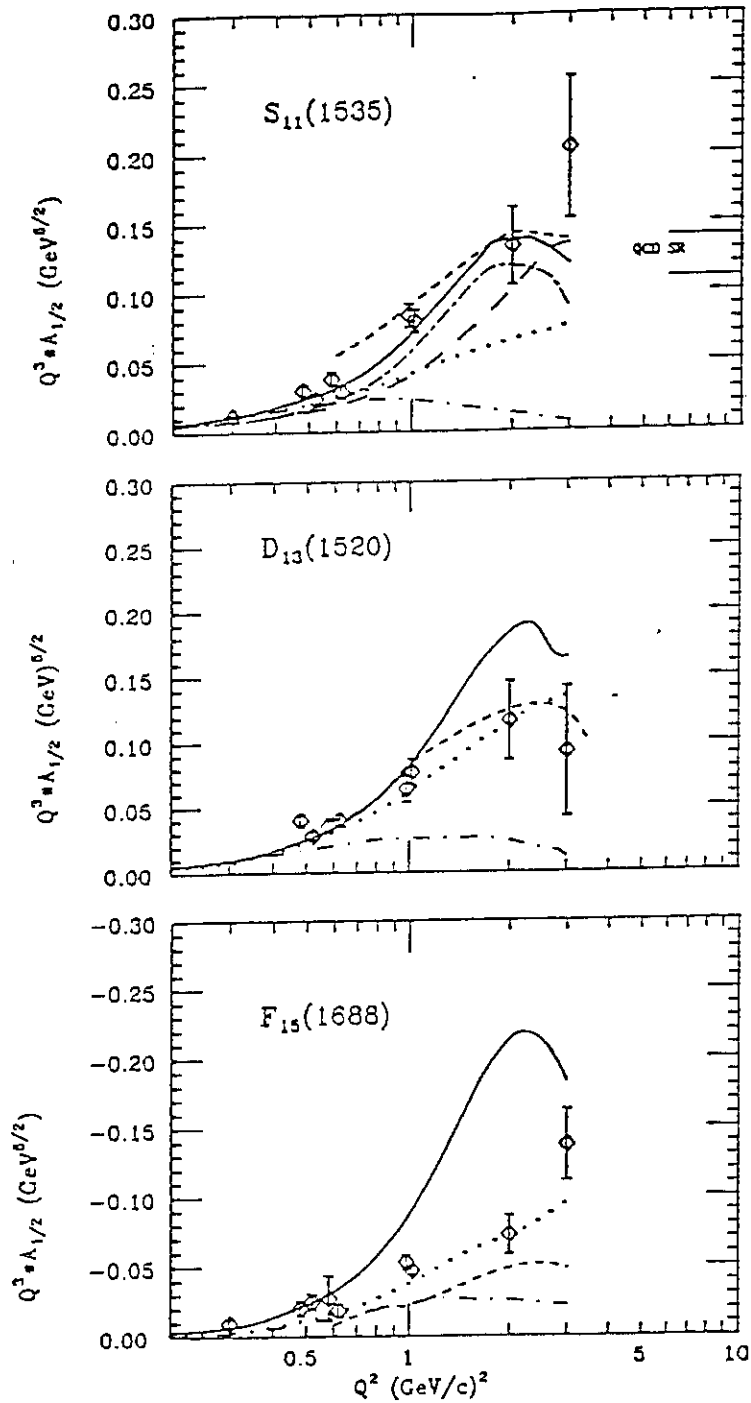


Figure 5.3  $Q^3 A_{1/2}$  for various resonance transitions. Same models as in Figure 4.4. The range of normalized QCD sum rule predictions of Carlson<sup>24</sup> for the asymptotic behavior of the  $\gamma_{\nu p} S_{11}$  transition are indicated lines labeled QCD SR.

led to renewed interest in experimental tests of the sum rule of Gerasimov<sup>58</sup> and Drell, and Hearn<sup>59</sup>, and in measurements of its  $Q^2$  evolution. The sum rule relates the difference in the total photo-absorption cross section on nucleons for photon-nucleon helicity  $\lambda_{\gamma N} = 1/2$  and  $\lambda_{\gamma N} = 3/2$  to the anomalous magnetic moment of the target nucleon:

$$\int_{\nu_{thr}}^{\infty} \frac{d\nu}{\nu} [\sigma_{1/2}(\nu, 0) - \sigma_{3/2}(\nu, 0)] = -\frac{2\pi^2\alpha}{M^2} \kappa^2 \quad (26)$$

where  $\nu$  is the photon energy,  $\sigma_{1/2}$  and  $\sigma_{3/2}$  are the absorption cross sections for total helicity 1/2 and 3/2, and  $\kappa$  is the anomalous magnetic moment of the target nucleon. The GDH sum rule has been derived on rather general grounds but has never been tested experimentally. There is however evidence from the analysis of single pion production that the sum rule cannot be grossly violated<sup>60</sup>.

The interpretation of the EMC results on the polarized proton structure functions in terms of the Bjorken sum rule<sup>61</sup> suggests the following behavior<sup>39</sup>:

$$\int_{\nu_{thr}}^{\infty} \frac{d\nu}{\nu} [\sigma_{1/2}(\nu, Q^2) - \sigma_{3/2}(\nu, Q^2)] \simeq \frac{0.134}{Q^2}. \quad (27)$$

The latter sum rule should be valid in the deep inelastic region. A comparison of (26) and (27) suggests that satisfaction of the GDH sum rule requires dramatic changes in the helicity structure of the  $\gamma p$  coupling between the deep inelastic region and  $Q^2 = 0$ . This is illustrated in Figure 5.4. A calculation by Anselmino et al.<sup>62</sup>, which is based on the vector meson dominance analogy shows a strong  $Q^2$  dependence and predicts significant uncertainty resulting from the assumed effective vector meson mass. In this calculation, the GDH limit  $-0.524 \text{ GeV}^{-2}$  at  $Q^2 = 0$  has been used for normalization. Calculations based on the more fundamental QCD sum rules should give a better understanding of the relation between the deep inelastic (asymptotic freedom) and the resonance (confinement) regimes. Such a calculation is now under way<sup>63</sup>. In addition, semi-empirical calculations based on a parametrization of the resonance photocoupling amplitudes and single quark transition model predictions are shown. Qualitatively, the change in helicity structure expected from the GDH sum rule limit and the deep inelastic EMC results is reproduced, with significant differences between the various calculations.

Figure 5.4 also shows the expected statistical error bars of the proposed CEBAF experiment to measure the GDH integral  $I_{GDH}(Q^2)$  for a mass cut-off at  $W \leq$

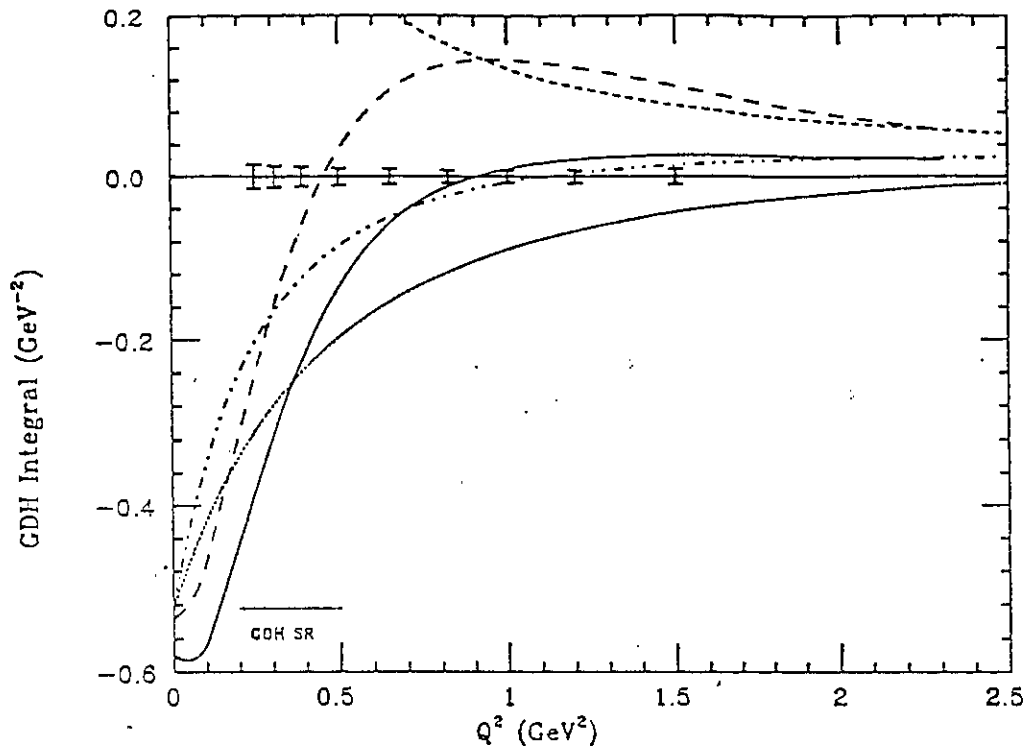


Figure 5.4 The GDH integral versus  $Q^2$  for various model calculations. The error bars indicate the expected statistical accuracy of the CEBAF experiment. The two lines around  $-0.58$  at  $Q^2=0.$ , were obtained with the AO code<sup>71</sup>: the solid line obtained with the Roper treated as a  $q^3G$  state, and the dashed line with it treated as a  $q^3$  object. The dash-dot-dot line and the dotted line use the form of Anselmino et al.<sup>62</sup> with the vector meson mass scale equal to  $m_\rho$  and to  $1.0$  GeV, respectively. The short dashed line represents eqn. (27)

$1.8\text{GeV}$ . Obviously, this experiment will make very significant contributions in the study of the  $Q^2$  evolution of the sum-rule, and to our understanding of the structure of the Roper resonance.

## 6. EXPERIMENTAL PROSPECTS

### 6.1 Single $\pi$ and $\eta$ Production

It is useful to distinguish baryon resonance studies according to the complexity of the final state. Most of the existing data consist of single  $\pi$  or  $\eta$  production. This channel is particular sensitive to the lower mass resonances ( $W \leq 1.7\text{GeV}$ ) which decay dominantly into the  $\pi N$  channel, or in the case of the  $S_{11}(1535)$  into  $\eta N$ . Much of the theoretical formalism required for data analysis has been worked out

for these channels. A thorough study of the lower mass region requires precise experimental studies of the single pseudoscalar meson channel. In single pion electroproduction from nucleons 11 independent measurements are needed at a given kinematical point  $Q^2$ ,  $W$ ,  $\theta_\pi$ , to determine the amplitudes of the process  $\gamma_e N \rightarrow N'\pi$  in a model independent fashion. The complete determination of the transition amplitudes in pion and eta production is a long term goal of nucleon resonance physics with electromagnetic probes. This program requires high statistics measurements of unpolarized cross sections, and detailed measurements of polarization observables using polarized beams, polarized nucleon targets, and the measurement of nucleon recoil polarization.

Measurement of the single pion cross section allows determination of the four response functions  $\sigma_T$ ,  $\sigma_L$ ,  $\sigma_{TT}$ ,  $\sigma_{LT}$  in (11), which are functions of the helicity amplitudes  $H_i$ . Measurement of polarization observables yield information on many response functions (table 6.1).

Experiment	# Response Functions
unpol. cross section	4
polarized e beam	1
polarized target	8
pol. beam/pol. target	5
recoil polarization	8
pol. beam/recoil pol.	5

Since polarization observables contain interference terms between amplitudes they are sensitive to small amplitudes and to relative phases between amplitudes. Information of limited statistical accuracy will prove extremely sensitive for determining absolute values and signs of small amplitudes which are otherwise not, or only with great difficulty, accessible.

Not all the response functions contain independent information. In particular, only four of the response functions measured with a polarized target are different

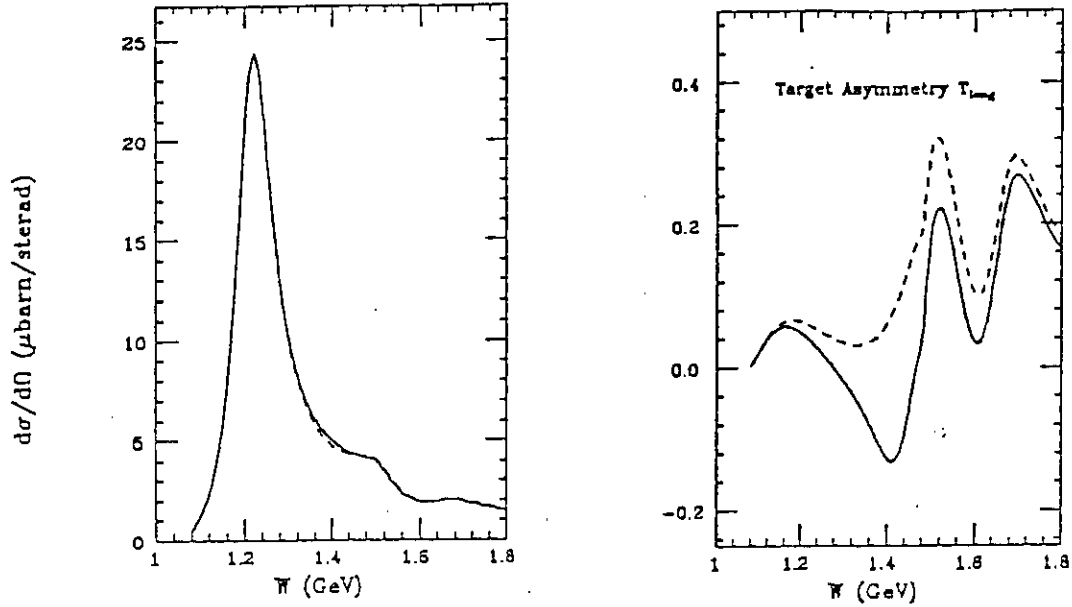


Figure 6.1 Predicted cross section (left) for  $\gamma_v p \rightarrow p\pi^0$  at  $Q^2 = 0.25\text{GeV}^2$ ,  $\epsilon = 0.8$ ,  $\theta_\pi^* = 90^\circ$ ,  $\phi_\pi = 30^\circ$ . The AO code<sup>71</sup> amplitudes were used. Predicted target asymmetry for target polarization along the incident electron beam  $T_{long}$  for the same kinematics (right). The sensitivity to the amplitudes of the Roper resonance is shown: solid line - with Roper, dashed line - without Roper.

from the ones measured with recoil polarimeters. In many applications the two methods can be quite competitive, which allows one to select the more convenient technique.

Figure 6.1 shows the sensitivity of the unpolarized cross section for  $p(e, e'p)\pi^0$  and the polarized target asymmetry  $T_{long}$  to the excitation strength of the Roper resonance  $P_{11}(1440)$ . As the transition amplitudes of the Roper may be quite small, the sensitivity of polarization experiments is essential in measuring these amplitudes. Similar sensitivities to the Roper amplitudes have been found for measurement of the proton recoil polarization<sup>64</sup> in  $p(e, e'\bar{p})\pi^0$ .

The main objective is to disentangle the various resonant partial waves. This requires measurement of complete angular distributions with respect to the direction of the virtual photon. Also, measurements in different isospin channels are needed to separate resonant and non-resonant amplitudes with different isospin assignments. Complete isospin information can be obtained from a study of the reactions

$$\gamma_v + p \rightarrow p + \pi^0$$

$$\gamma_v + p \rightarrow n + \pi^+$$

$$\gamma_v + n \rightarrow p + \pi^-$$

In addition, measurement of

$$\gamma_v + p \rightarrow p + \eta$$

selects isospin 1/2, and is a unique means of tagging the  $S_{11}(1535)$  and the  $P_{11}(1710)$  resonances.

The various experimental requirements call for an experimental setup which allows measurement of complete angular distributions in different isospin channels simultaneously.

## 6.2 Multiple Pion Production.

For higher masses, multiple pion production due to decay channels like  $\Delta\pi$ ,  $\rho N$ , and  $\omega N$  becomes the dominant process. For example, the  $S_{31}(1650)$  or  $D_{33}(1700)$  are known to decay to about 70% or 85%, respectively into the  $N\pi\pi$  channel, with dominant contributions coming from the  $\pi\Delta(1232)$  decay. Obviously, a study of baryon resonance production in this mass region requires measurement of these channels.

The information that can be extracted from the two-pion process is much richer than in the single pion case since polarization observables can be measured in the final state. For example, the measurement of the  $\Delta \rightarrow N\pi$  decay allows a determination of the  $\Delta$  polarization in the process  $\gamma p \rightarrow \Delta\pi$ . This should prove very powerful in determining the resonant contributions to the process. Moreover, the search for the higher gluonic state candidates  $P_{13}(1540)$  and  $P_{31}(1550)$ , and, if found, the measurement of their photocoupling amplitudes also appears more promising in the multi-pion channel than in single pion production.

## 6.3 Experimental Equipment

A comprehensive and efficient experimental program to study electromagnetic transitions of baryon resonances in a large kinematical region, calls for experimental equipment with large solid angle coverage, capable of measuring neutral particles, and compatible with polarized proton and neutron targets. At CEBAF, a large acceptance spectrometer (CLAS) based on a toroidal magnetic field is being built<sup>1</sup>. A large portion of the scientific program for this detector is aimed at studies of baryon resonance excitations using electron beams<sup>36</sup>. Figure 6.2 shows an artists view of the CLAS spectrometer.

Many details of baryon resonance excitations, in particular at lower masses, may be addressed with magnetic spectrometers, which have small solid angles, but

are able to operate at very high luminosities. Single pion production near pion threshold and in the  $\Delta(1232)$  region, or eta production in the  $S_{11}(1535)$  region could be measured with high precision. Small solid angle, high rate magnetic spectrometers may also allow accurate measurements of proton recoil polarizations in reactions such as:

$$e + p \rightarrow e + \bar{p} + \pi^0$$

$$e + n \rightarrow e + \bar{p} + \pi^-$$

$$e + p \rightarrow e + \bar{p} + \eta.$$

Polarization experiments with such spectrometers are in preparation at CEBAF, at MIT-Bates<sup>37</sup>, and at MAMI-B<sup>65</sup>. These are designed to make precise measurements of single  $\pi^0$  production off protons in the  $\Delta(1232)$  region, with the goal of extracting more accurate information about the small  $E_{1+}$  and  $S_{1+}$  multipoles.

## 7. OUTLOOK

In spite of the enormous effort that has already gone into the study of hadronic properties of matter using hadron beams, the field of light quark baryon spectroscopy appears to be still in its infancy. This is due to several factors. First, theoretical guidance based on models which have some relationship to the theory of strong interaction QCD was established only after the bulk of the experiments had been completed. Second, all of the high statistic experiments are single pion production measurements. In view of QCD based quark models, this allows the study of lower mass states with a large elasticity. However, single pion production measurements are not suited for the study of most of the higher mass states. These are predicted to largely decouple from the  $\pi N$  channel, which makes this channel less and less sensitive to resonance excitation in the higher mass region. Third, with the exception of low energy machines such as LAMPF, there are presently no hadron machines available where these experiments could be done in an efficient way. Fortunately, the prospects for the construction of the hadron machine KAON in Canada have improved recently, and one may hope that adequate equipment for multi-meson production experiments will be implemented.

The electromagnetic measurements suffered from the same shortcomings. In addition, the notorious rate problem in electroproduction experiments prevented high statistics experiments from being carried out, even for single pion production. Fortunately, the prospects in this sector are indeed excellent. Several new CW electron

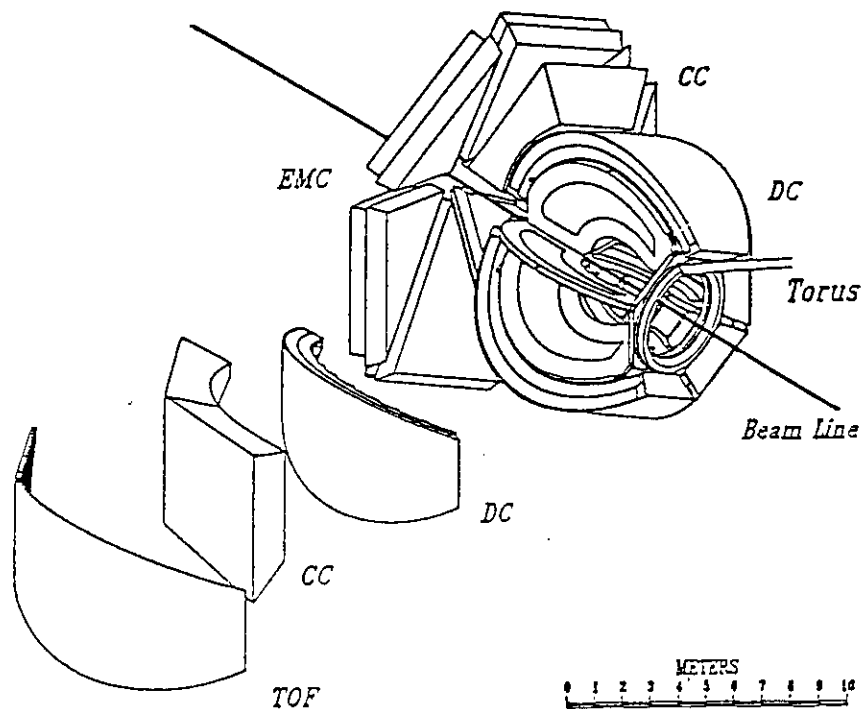


Figure 6.2 The CEBAF Large Acceptance Spectrometer (CLAS)<sup>1</sup>. Six symmetrically arranged superconducting coils generate an approximate toroidal magnetic field. Drift chambers, time-of-flight counters, gas Cerenkov counters, and an electromagnetic calorimeter provide particle identification, charged particle tracking, and energy measurements for electromagnetic particles. The field free region around the target allows use of polarized solid state targets.

accelerators in the GeV and multi-GeV range are now under construction. Figure 7.1 shows the resonance mass range accessible with these machines. Clearly, with these machines, and with the use of modern experimental equipment, the scientific community will have powerful new instruments, which will allow an onslaught on many of the outstanding problems in baryon structure and strong interaction physics.

#### ACKNOWLEDGEMENTS

I wish to thank Ralph Minehart for a critical reading of the manuscript and useful comments.

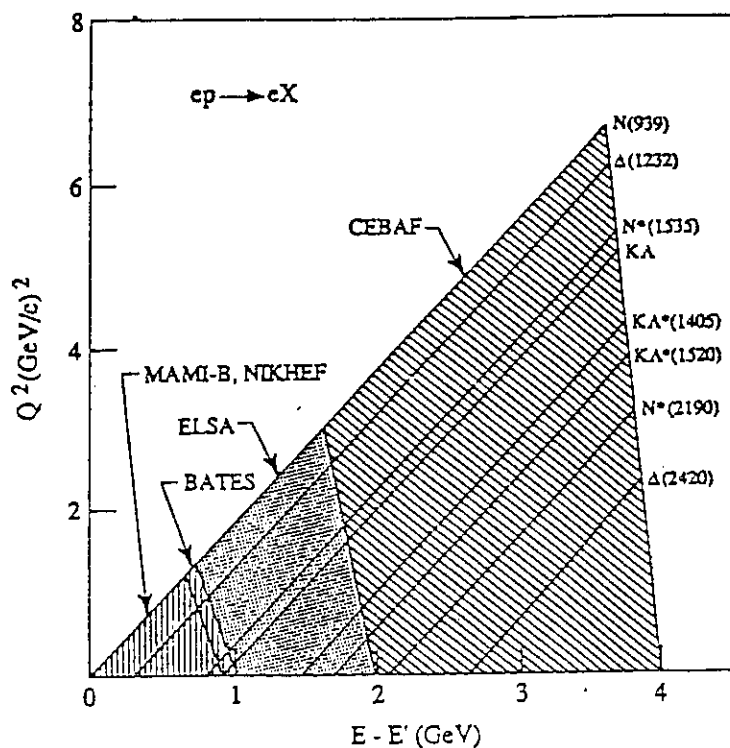


Figure 7.1 Kinematical region accessible at various CW electron machines.

#### References.

- [1] V. Burkert and B. Mecking, Large Acceptance Detectors for Electromagnetic Nuclear Physics, in: Modern Topics in Electron Scattering, eds. B. Frois, I. Sick, World Scientific, Singapore.
- [2] Particle Data Group, Review of Particle Properties, Phys. Lett. B239 (1990)
- [3] G. Höhler, Nucl. Phys. A508 (1990), 525
- [4] N. Isgur, G. Karl, Phys. Lett. 72B, 109 (1977); Phys. Rev. D23, 817 (1981).
- [5] S. Capstick, N. Isgur, Phys. Rev. D34, 2809 (1986); S. Capstick, Phys. Rev. D36, 2800 (1987)
- [6] D. Menze, Excited Baryons 1988, Troy, NY, 1988, World Scientific Publisher, eds. G. Adams, et al.
- [7] C. Forsyth, R. Cutkosky, Z. Phys. C18, 219 (1983)
- [8] D. Bugg, Phase Locking of Resonances, Talk presented at the conference on 'Excited Baryons 88', Troy, NY, 1988.
- [9] R. Koch, E. Pietarinen, Nucl. Phys. A336, 331 (1980). Höhler, Landolt-Börnstein I/9b2, Springer Verlag (1983)
- [10] R.E. Cutkosky et al., Phys. Rev. D20, 2839 (1979)

- [11] R.A. Arndt, J.M. Ford and L.D. Roper, Phys. Rev. D32, 1085 (1985)
- [12] R.E. Cutkosky, Proc. 2nd International Workshop on  $\pi N$  Physics (1987), Los Alamos Report, LA-11184-C, pg. 167
- [13] For an overview see: M.E. Sadler, Proc. 2nd International Workshop on  $\pi N$  Physics (1987), Los Alamos Report, LA-11184-C, pg. 200
- [14] R. Koniuk, N. Isgur, Phys. Rev. D21, 1868 (1980)
- [15] D.M. Manley et al., Phys. Rev. D30, 904 (1984)  
D. M. Manley, Phys. Rev. Lett. 52, 2122 (1984)
- [16] K.F. Liu, C.W. Wong, Phys. Rev. D28, 170 (1983)
- [17] F. Iachello, Phys. Rev. Lett. 62, 2440 (1989)
- [18] E. Golowich, E. Haqq, G. Karl, Phys. Rev. D28, 160 (1983)
- [19] T. Barnes, F.E. Close, Phys. Letts. 123B, 89 (1983).
- [20] R. Longacre, Nucl. Phys. B211, 1 (1977)
- [21] Z.P. Li, Phys. Rev. D44, 2841(1991)
- [22] Z.P. Li, V. Burkert, Z. Li, Electroproduction of the Roper Resonance as a Hybrid State, Preprint CEBAF-PR-91-032.
- [23] M. Köbberling, et al., Nucl. Phys. B82, 201 (1974)  
S. Stein et al., SLAC-PUB-1518 (1975)
- [24] C.E. Carlson, Phys. Rev. D34, 2704 (1986)  
C.E. Carlson, J.L. Poor, Phys. Rev. D38, 2758 (1988)  
C.E. Carlson, Proc. 12th Internat. Conf. on Few Body Problems in Physics, Vancouver, July 2-8, 1989.
- [25] P. Stoler, Phys. Rev. Lett. 66, 1003 (1991)
- [26] K. Bätzner et al., Phys. Lett. 39B, 575 (1972)
- [27] J. Drees et al., Z. Phys. C7, 183 (1981)
- [28] H.F. Jones and M.D. Scandron, Ann. Phys. 81, 1 (1972)
- [29] M. Warns et al., Z. Phys.C45, 627 (1990)
- [30] G. Baum et al.; Phys. Rev. Lett. 45, 2000 (1980);
- [31] V. Burkert et al., CEBAF Proposal PR-91-023
- [32] F. Foster and G. Hughes, Rep. Prog. Phys., Vol. 46, 1445 (1983)
- [33] V. Eckardt, et al., Nucl. Phys. B55, 45(1973)  
K. Wacker et al., Nucl. Phys. B144, 269 (1978)
- [34] R.L. Walker, Phys. Rev. 182, 1729 (1969)
- [35] G. Eckart and B. Schwesinger , Nucl. Phys. A458, 620 (1986)
- [36] W. Albrecht et al., Nucl. Phys. B27, 615 (1971)  
S. Galster et at., Phys. Rev. D5, 519 (1972)

- R. Siddle et al., Nucl. Phys. B35, 93 (1971)  
 R. D. Hellings et al., Nucl. Phys. B32, 179 (1971)  
 J.C. Alder et al., Nucl. Phys. B46, 573 (1972)  
 K. Bätzner et al., Nucl. Phys. B75, 1 (1974)
- [37] R. Lourie, et al., Bates Proposal PR 89-03;  
 C. Papanicolas et al., Bates Proposal PR 87-09.
- [38] V. Burkert, et al., CEBAF Proposals of the  $N^*$  collaboration.
- [39] F.E. Close, Proc. Int. Conf. Excited Baryons 1988, Troy, NY, 1988, World Scientific Publisher, eds. G. Adams, et al.
- [40] K. Bermuth, D. Drechsel, D. Tiator and J.B. Seaborn, Phys. Rev. D37, 89 (1988)
- [41] L.A. Copley, G. Karl, E. Obryk, Phys. Letts. 29B, 117 (1969)
- [42] F. Foster, G. Hughes, Z. Phys. C14, 123 (1982)
- [43] F. Close and Z.P. Li, Phys.Rev.D42, 2194(1990)
- [44] W. Konen and H.J. Weber, Phys. Rev. D41, 2201 (1990)
- [45] C.P. Forsyth, J.B. Babcock, Preprint CMU-HEP 83-4 (1983)
- [46] F.E. Close, F.J. Gilman, Phys. Letts. 38B, 541 (1972)  
 F.E. Close, F.J. Gilman, I. Karliner, Phys. Rev. D6, 2533 (1972)
- [47] A.J.G. Hey, J. Weyers, Phys. Letts. 48B, 69 (1974)
- [48] S. Ono, Nucl. Phys. B107, 522 (1976)
- [49] W.N. Cottingham, I.H. Dunbar, Z. Phys. C2, 41 (1979)
- [50] H. Breuker et al., Z. Phys. C17, 121 (1983)  
 H. Breuker et al., Z. Phys. C13, 113 (1982)
- [51] V. Burkert, Proceedings, 18th Rencontre de Moriond, January 23-29, 1983, La Plagne, pg. 189, Editions Frontières, ed. J. Tran Thanh Van.
- [52] H. Funsten et al. CEBAF Proposal 91-024 (1991)
- [53] D. Menze, Talk presented at the Int. Workshop on Baryon Structure and Spectroscopy, Paris, September 22-25, 1991.
- [54] S.J. Brodsky, G.P. Lepage, Phys. Rev. D24, 2848 (1981).
- [55] N. Isgur and C.H. Llewellyn-Smith, Nucl. Phys. B317, 526 (1989)
- [56] R.P. Feynman, Photon Hadron Interactions, Frontiers in Physics, W.A. Benjamin, Inc. (1972), pg.49.
- [57] J. Ashman et al., Phys. Lett. 206B, 364(1988)
- [58] S. Gerasimov; Yad. Fiz. (1965), Soviet J. Nucl. Phys. 2, 930 (1966)
- [59] S.D. Drell and A.C. Hearn; Phys. Rev. Lett. 16, 908 (1966)
- [60] I. Karliner, Phys. Rev. D7, 2717(1973)

- [61] J.D. Bjorken; Phys. Rev. 148, 1467 (1966)
- [62] M. Anselmino, B.L. Ioffe, E. Leader, Sov. J. Nucl. Phys. 49, 136(1989)
- [63] A. Radyushkin, private communications
- [64] R. Lourie, Z. Phys. C50, 345 (1991)
- [65] Reports on Research Activities in Nuclear Physics, 1990 Photonuclear Gordon Conference.
- [66] C. Gerhardt, Z. Phys. C4, 311(1980)
- [67] H. Breuker et al., Phys. Letts. 74B, 409 (1978)
- [68] W. Brasse et al., Z. Phys. C22, 33 (1984)
- [69] R.C.E. Devenish, T.S. Eisenschitz, J.G. Körner, Phys. Rev. D14, 3063 (1976)
- [70] R.G. Moorhouse, in: Electromagnetic Interactions of Hadrons, Vol. 1, pg. 83, eds. A. Donnachie, G. Shaw, Plenum Press, 1978.
- [71] V. Burkert, Zh. Li, Computer code AO, unpublished.